CHAPTER 5

MINERALOGY

In this chapter, detailed mineralogical data on the constituent mineral phases of the tholeiitic rocks are reported and discussed in relation to the chemistry of their respective host rocks and their environment of crystallization. Particular attention is devoted to the pyroxenes and feldspars, which constitute the major part of the mode of most of the rocks, with proportionately less emphasis on the olivines, opaque oxides and accessory phases.

Details of the analytical conditions and the instrument employed for the microprobe analyses are outlined in Appendix I.

5.1 OLIVINE

Olivine as phenocrysts or microphenocrysts occurs in many rocks and is ubiquitous as a groundmass constituent throughout the low-Si series. In the high-Si series it commonly occurs as sparse phenocrysts but in the groundmass its place is taken by Ca-poor pyroxene (usually pigeonite).

Microprobe analyses of olivines are set down in Tabe II.1 (Appendix II) together with structural formulae and 100 Mg/Mg+Fe (=Mg-value = m) ratios. Cation summations indicate that all analyses are quite satisfactory. Unfortunately the microprobe was not programmed to analyse for Ni. Other minor elements reported in olivine analyses (notably Ti and Al) are below the limits of sensitivity.

In the low-Si series, olivine phenocrysts are particularly common in the more Mg-rich representatives and there is a general decrease in size,

abundance and Mg content with increasing Fe/Mg of the host rock (Fig. 5.1). Groundmass olivines are significantly enriched in iron relative to early-formed phenocrysts and show minimal compositional variation.

In the high-Si series, olivine crystallized early as sparse phenocrysts, now mantled by Ca-poor pyroxene (pigeonite) excepting the most iron-rich phenocrysts. Commonly phenocrysts are partially or completely pseudomorphed by bowlingite leaving a relict mantle of pigeonite. Iron-rich olivine phenocrysts are partly altered to red-brown iddingsite.

Only limited microprobe data are available on olivines in the high-Si series (Fig. 5.1). However the available data again suggest strong dependence of composition on the Fe/Mg ratio of the host. The olivines of the icelandite 28071 appear anomolously Mg-rich in relation to their host rock. However the rock displays abundant evidence of mixing of magmas (Chapter 7) and it is therefore unlikely that these olivines were in equilibrium with the host liquid.

Discussion of olivine crystallization in relation to the pyroxenes and aspects of the olivine Ca-poor pyroxene-liquid relationship are discussed later in conjunction with pyroxene crystallization.

MINOR ELEMENTS IN OLIVINE

Minor element microprobe data for CaO and MnO are plotted in Figure 5.2 against olivine Mg-values.

Mn shows typical variation in increasing with decreasing Mg (Simkin and Smith, 1970; Moore and Evans, 1967). No real difference in the behaviour of Mn is evident between olivines of the two series. Entry

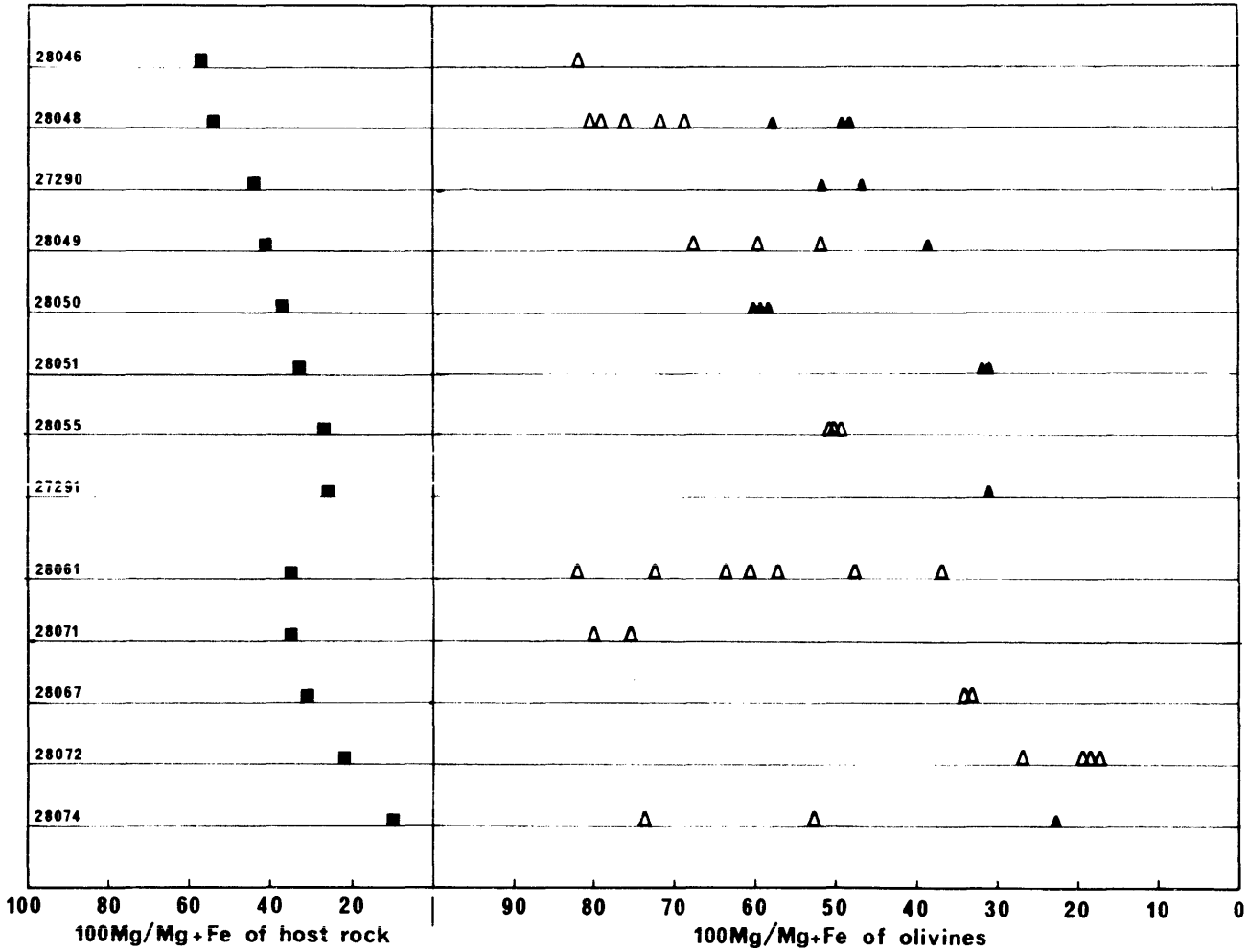

Fig. 5.1: Diagram illustrating the relationship between the 100 Mg/Mg+Fe (atomic) ratios of olivines and their respective host rocks. Squares, host rocks; open triangles, olivine phenocrysts; small triangles, groundmass olivines.

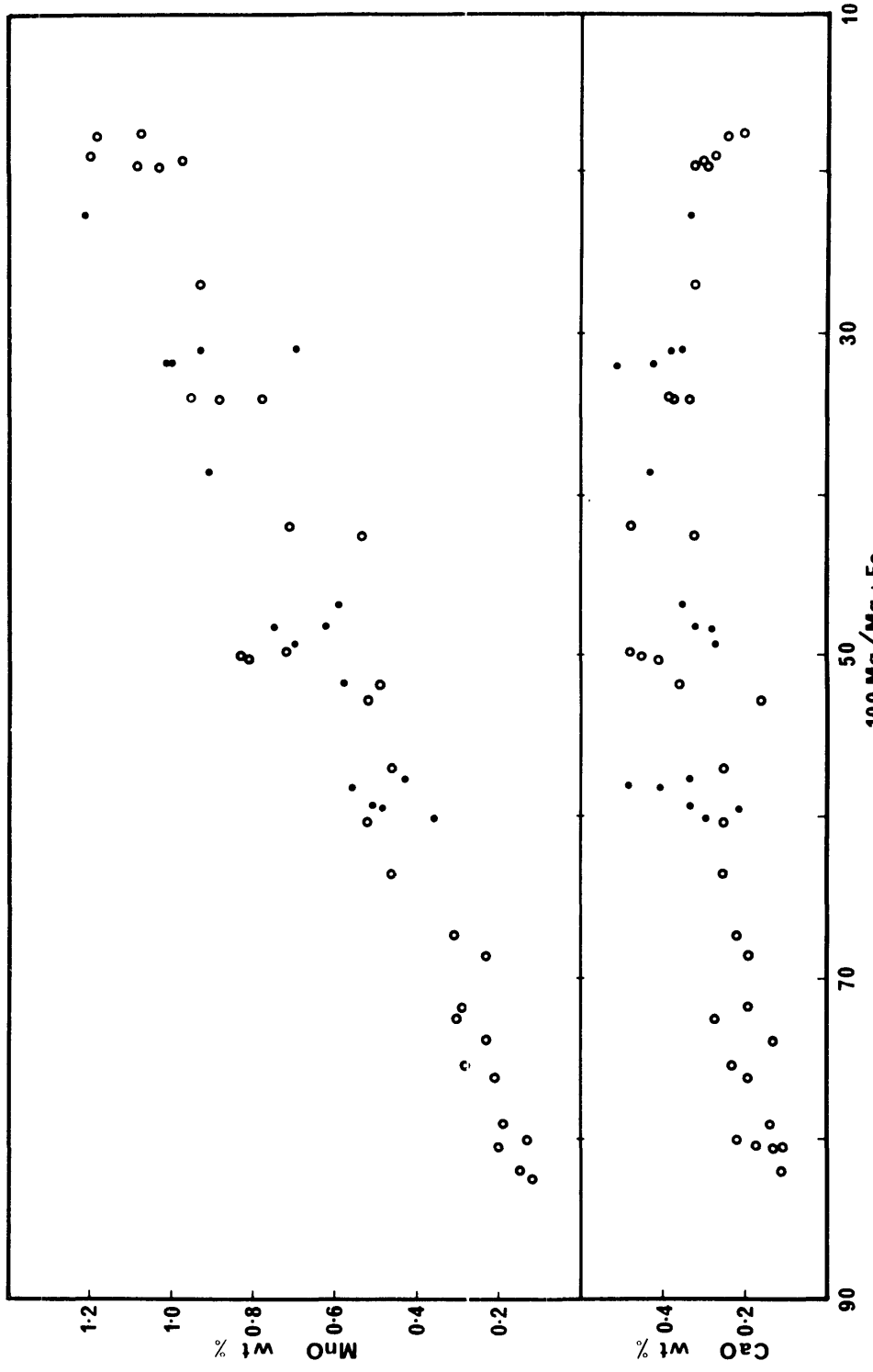

Fig. 5.2: Plots of CaO and MnO (wt %) against the 100 Mg/Mg+Fe (atomic) ratios of analysed olivines. Open circles, olivine phenocrysts; filled circles, groundmass olivines.

of Mn into olivine is probably a function of host rock composition rather than any particular physico-chemical conditions at the time of crystallization.

Ca content increases with decreasing Mg-value to about Fo_{30} and thereafter decreases. Entry of Ca into olivine has been discussed in some detail by Simkin and Smith (1970) and Stormer (1973). Simkin and Smith interpret a distinct correlation between Ca content of olivine and crystallization history as indicating pressure dependence. Thus olivines from a plutonic environment almost invariably contain less than 0.1% CaO while hypabyssal and volcanic olivines are somewhat richer in CaO. Stormer (1973) demonstrated additional strong dependence of Ca content on silica activity in the host magma, itself somewhat pressure dependent (Nicholls *et al.*, 1971), by recourse to thermodynamic considerations and natural examples from rocks with varying degrees of silica saturation. He shows that in undersaturated (ne normative) rocks, olivine phenocryst margins and groundmass grains are strongly enriched in Ca relative to phenocryst interiors whereas marginal enrichment in Ca is minimal in oversaturated rocks.

The increasing Ca with decreasing Mg exhibited by both phenocryst and groundmass grains in the range Fo_{82} to Fo_{30} suggests additional dependence of Ca content on Fe content of olivines as neither of the above processes explain this trend. It is apparent that while silica activity and pressure are undoubtedly important controlling factors governing the entry of Ca into olivine, other factors such as Mg/Fe ratio of the olivine and availability of Ca in the host liquic cannot be ignored.

5.2 PYROXENES

Pyroxenes occur in most basic and intermediate tholeiitic rocks of the Tweed Shield. Augite is present in almost all low-Si tholeiitic andesites as a groundmass phase and but is very rare as phenocrysts. On the other hand, in the high-Si series augite is a common phenocryst and groundmass phase in rocks from tholeiitic andesite through to tholeiitic rhyodacite. Hypersthene and pigeonite are restricted solely to the high-Si series where both are common phenocryst species; pigeonite is also ubiquitous as a groundmass phase in the high-Si series. Ferrohypersthene-eulite occurs as phenocrysts in many rhyolitic pitchstones. Aluminian bronzite and subcalcic augite, interpreted as high pressure cognate phases, occur in some tholeiitic andesites of the low-Si series (Duggan and Wilkinson, 1973).

Some one hundred and twenty microprobe analyses of pyroxenes have been obtained and these are tabled along with their structural formulae in Appendix II. The data listed therein have been used in Figures 5.3 to 5.13.

5.2.1 Pyroxenes of the Low-Si Series

(i) High Pressure phenocrysts (Megacrysts)

A discussion on the occurrence of high pressure pyroxenes in a high-alumina tholeiitic andesite (27290; Al_2O_3 = 18.45%) has already been presented (Duggan and Wilkinson, 1973). Similar phases are also found occasionally in other low-Si tholeiitic andesites with more normal Al_2O_3 contents (13-15%).

Aluminian bronzite is always the dominant pyroxene megacryst phase, exceeding subcalcic augite; the bronzite is invariably surrounded by a reaction rim of granular olivine wherever it has been in direct contact with host liquid. These aluminian pyroxenes invariably coexist with plagioclase, also suspected to be a high pressure phase. These feldspars commonly show a characteristic sieved reaction rim surrounding a relatively sodic unzoned core and narrow mantle of more calcic plagioclase.

The chemistry of pyroxene megacrysts for which microprobe data are available has already been discussed and will not be further considered here. The significance of high pressure processes in the genesis of their host lavas and other lavas of the shield will be fully considered in Chapter 7.

(ii) Low Pressure Phenocrysts

Pyroxene is rarely an early phase in the low-Si series. However in one analysed Fe-rich tholeiitic andesite (28055) from a flow near Alstonville, phenocrysts of augite and rare olivine occur together with plagioclase and titanomagnetite in a groundmass heavily charged with opaque oxides. This particular rock, rich in iron and alkalis, will be interpreted as a relatively evolved low pressure differentiate of the more typical mafic low-Si tholeiitic andesite magma.

The augite phenocrysts are prismatic, up to 0.5 mm in length and pale brown in colour. They show little chemical variation in terms of either Ca, Mg, and Fe (Fig. 5.4) or the minor elements Al, Ti and Na (Table II.2a; Anals. 24 to 33). On rare occasions phenocrysts exhibit

weakly developed hour glass zoning. Microprobe data on one such phenocryst indicates relatively higher Ti and Al and lower Si in the relatively dark brown zones.

(iii) Groundmass Pyroxenes

Ca-rich pyroxene is a groundmass phase in a majority of low-Si tholeiitic andesites. More rarely pyroxene occurs only as feathery aggregates within the iron-rich residual glass, a common feature of many tholeiitic lavas of the Inverell area, N.S.W. (Wilkinson and Duggan, 1973). Groundmass pyroxenes vary in habit from sub-ophitic to intergranular, the latter being more common in rocks with a finer grained groundmass. They are usually colourless to very pale mauve or smokey brown in colour.

Detailed scanning of groundmass pyroxenes by the electron microprobe failed to reveal any evidence of mantling of augite by a Ca-poor pyroxene or zoning to significantly more subcalcic compositions.

Groundmass pyroxene compositions for several low-Si tholeiitic andesites are listed in Table II.2a (Appendix II). A collation of these data are illustrated in Figure 5.3; plots of pyroxenes from individual rocks are shown in Figure 5.4. Variation within individual flows is quite small but the overall variation in Fe/Fe+Mg ratios reflects variable Fe/Fe+Mg ratios of the host rocks. Selected analyses, chosen to illustrate principal compositional features of the pyroxenes are listed in Table 5.1.

Figure 5.4 reveals an interesting trend of increasing Ca with increase in Fe/Fe+Mg ratios. This is the reverse of the trend observed in the pyroxenes of slowly cooled tholeiitic intrusions such as Skaergaard (Brown, 1957,1967), Bushveld (Atkins, 1969) and Red Hill, Tasmania (McDougall,

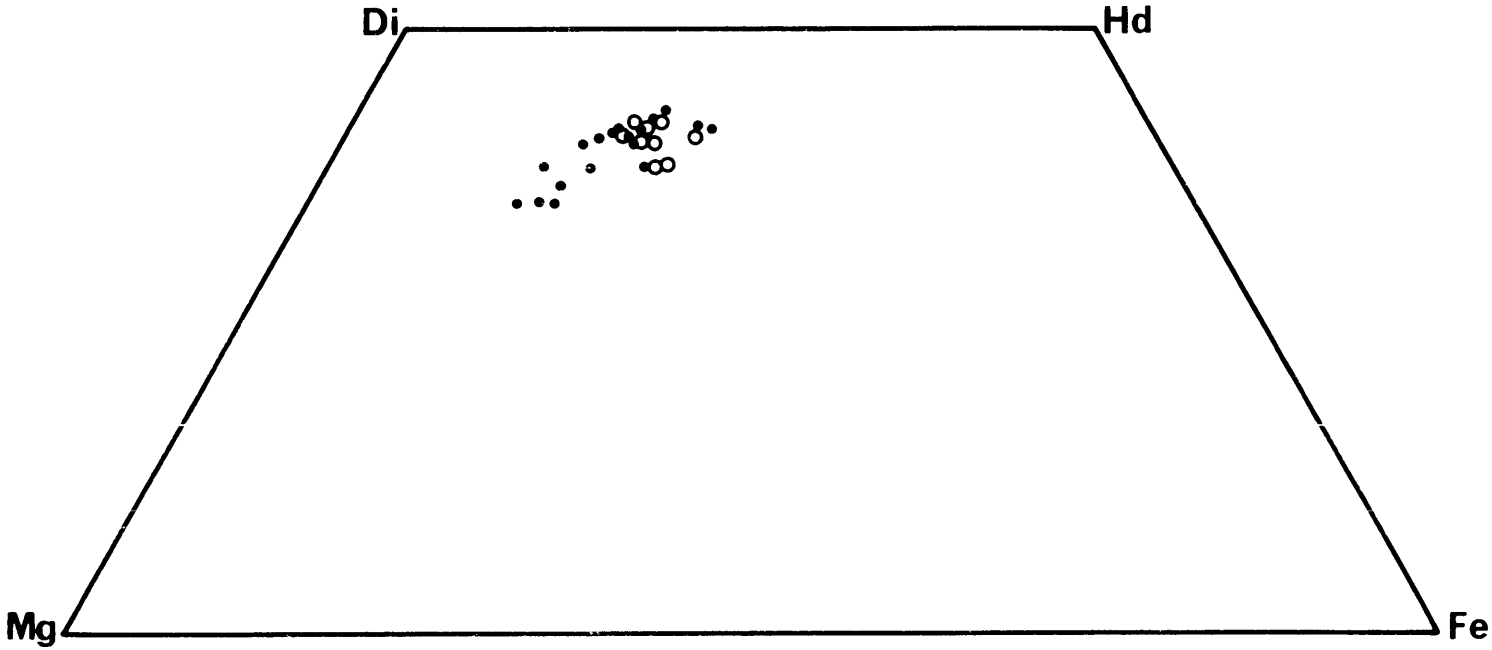

Fig. 5.3: Collation of microprobe data on low pressure pyroxenes from rocks of the low-Si series plotted in terms of Ca, Mg and Fe (atom %) in the conventional pyroxene quadrilateral. Open circles, pyroxene phenocrysts; filled circles, groundmass pyroxenes.

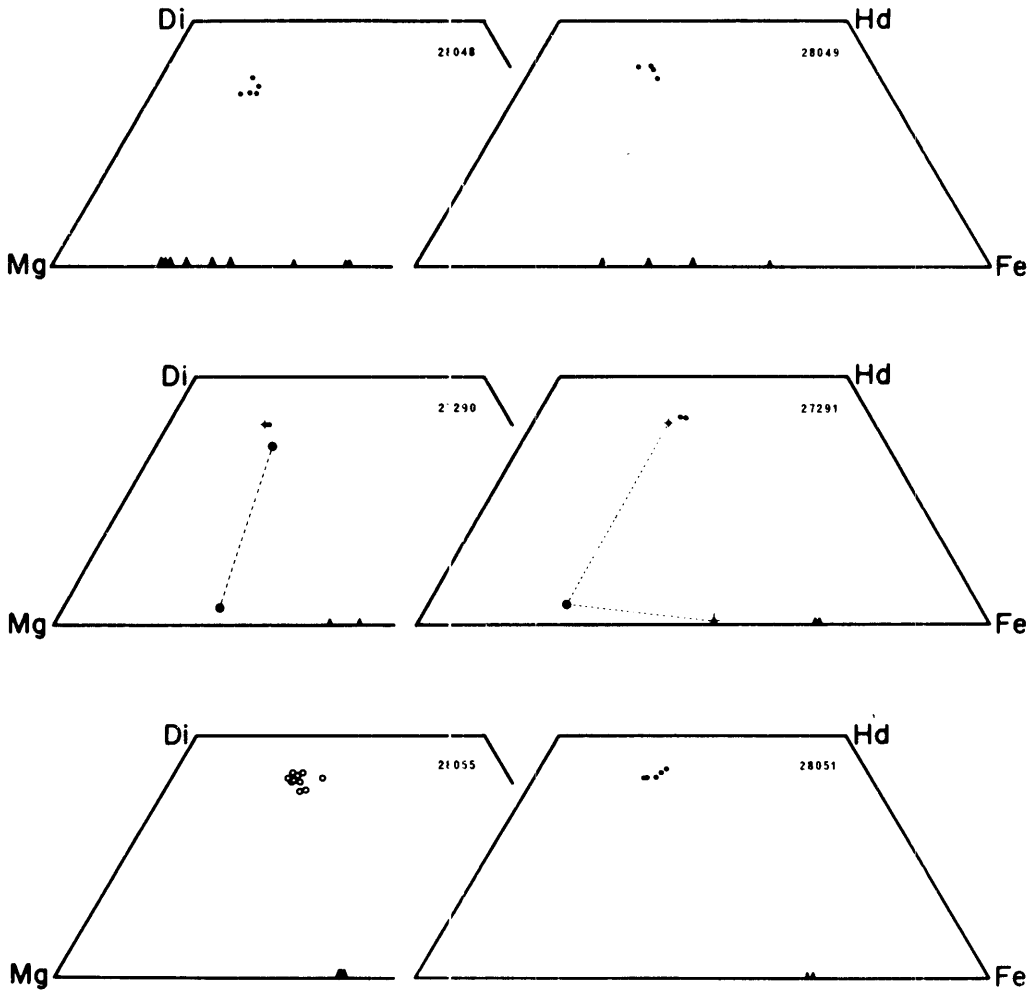

Fig. 5.4: Analysed pyroxenes and olivines from individual rocks of the low-Si series plotted in terms of Ca, Mg and Fe (atom %) in the conventional pyroxene quadrilateral. Open circles, low pressure pyroxene phenocrysts; filled circles, groundmass pyroxenes; ⊕, high pressure pyroxene megacrysts; ✦, pyroxene from reaction rim to pyroxene megacryst; large triangles, olivine phenocrysts; small triangles, groundmass olivines; ✦, olivine from reaction rim to pyroxene megacryst. Tie lines join coexisting high pressure pyroxenes and their reaction products.

TABLE 5.1

SELECTED MICROPROBE ANALYSES OF LOW PRESSURE PHENOCRYST AND GROUNDMASS PYROXENES FROM MEMBERS OF THE LOW-Si SERIES

	1	2	3	4	5	6	7
SiO_2	51.16	51.03	51.85	50.17	50.53	51.61	51.08
TiO_2	0.73	0.77	1.14	1.37	1.30	0.99	0.79
Al_2O_3	1.63	1.91	2.15	2.57	2.16	1.81	1.83
FeO^{*3}	14.51	13.07	11.04	12.76	12.95	11.80	15.07
MnO	0.40	0.27	0.32	0.25	0.26	0.22	0.31
MgO	13.06	13.14	15.68	13.00	12.14	14.73	11.09
CaO	18.53	19.41	17.82	19.01	20.25	18.62	19.71
Na_2O	0.21	0.52	0.44	0.37	0.28	0.18	0.15
Total	100.23	100.12	100.42	99.50	99.87	99.96	100.03
Si	1.939	1.930	1.925	1.906	1.920	1.935	1.949
Al^{IV}	0.061	0.070	0.075	0.094	0.080	0.065	0.051
Al^{VI}	0.012	0.015	0.019	0.021	0.017	0.015	0.031
Ti	0.021	0.022	0.032	0.039	0.037	0.028	0.023
Fe^{2+}	0.460	0.413	0.342	0.405	0.411	0.370	0.481
Mn	0.013	0.009	0.010	0.008	0.008	0.007	0.010
Mg	0.738	0.741	0.868	0.736	0.687	0.823	0.631
Ca	0.752	0.787	0.709	0.774	0.824	0.748	0.806
Na	0.015	0.038	0.031	0.027	0.020	0.013	0.011
Σ xy	2.01	2.03	2.01	2.01	2.00	2.00	1.99
Ca	38.6	40.5	37.0	40.4	42.9	38.5	42.0
Mg	37.8	38.2	45.2	38.4	35.7	42.4	32.9
Fe	23.6	21.3	17.8	21.2	21.4	19.1	25.1
$\frac{100\ Fe}{Fe+Mg}$	38.4	35.8	28.3	35.6	37.5	31.1	43.3

KEY TO TABLE 5.1

Selected analyses of low-pressure phenocryst and groundmass pyroxenes from members of the low-Si series.

1) Core of augite phenocryst in Fe-rich low-Si tholeiitic andesite 28055 (Table II.2a, Anal. 24).

2) Rim of augite phenocryst in Fe-rich low-Si tholeiitic andesite 28055 (Table II.2a, Anal. 26).

3) Groundmass augite in low-Si tholeiitic andesite 28048 (Table II.2a, Anal. 1).

4) Groundmass augite in low-Si tholeiitic andesite 28049 (Table II.2a, Anal. 8).

5) Groundmass augite in low-Si tholeiitic andesite 28051 (Table II.2a, Anal. 14).

6) Groundmass augite in high-Al low-Si tholeiitic andesite 27290 (Table II.2a, Anal. 19).

7) Groundmass augite in Fe-rich low-Si tholeiitic andesite 27291 (Table II.2a, Anal. 22).

1961) and in various tholeiitic volcanic series, e.g. Thingmuli (Carmichael, 1967a). It also differs from the established crystallization trend of clinopyroxenes for undersaturated basaltic magmas (Wilkinson, 1957; Brown 1967) which, like the Tweed low-Si series, lack a coexisting Ca-poor pyroxene phase.

Among minor elements in the pyroxene structure, only Ti,Al,Mn, and Na are significant in these particular pyroxenes.

Substitution of Al has been appreciable. The Al_2O_3 content of the groundmass pyroxenes varies from 1.5 to 3.5%, somewhat higher than generally recorded for tholeiitic rocks of comparable silica saturation. For example, Thingmuli Ca-rich pyroxenes in rocks with minor qz average 1.0-2.0% Al_2O_3 and an augite from the Red Hill quartz dolerite contains 1.6% Al_2O_3 (McDougall, 1961). Structural formulae of the Tweed pyroxenes calculated on the basis of 6 oxygen atoms indicate that most of the Al is in the z site, with Al^{IV} in the range 0.050-0.108 atoms. Al^{VI} is usually less than 0.025, with rare examples somewhat higher.

Ti substitution shows a positive correlation with Al content and in particular with Al^{IV}. Figures 5.5a and 5.5b illustrate $Al^{(total)}$ vs Ti and Al^{IV} vs Ti respectively. The line aa' corresponds to an Al:Ti ratio of 2:1. The close proximity of the analyses to aa' in Figure 5.5b indicates the importance of the $CaTiAl_2O_6$ "component" (so-called "titanpyroxene"; Yagi and Onuma, 1967) in this substitution at low pressures (Gupta *et al.*, 1973). The excess Al over this ratio in Figure 5.5a mainly represents the contribution of Ca-Tschermak's component ($CaAl_2SiO_6$) to the composition, discussed more fully in relation to the pyroxenes of high-Si series.

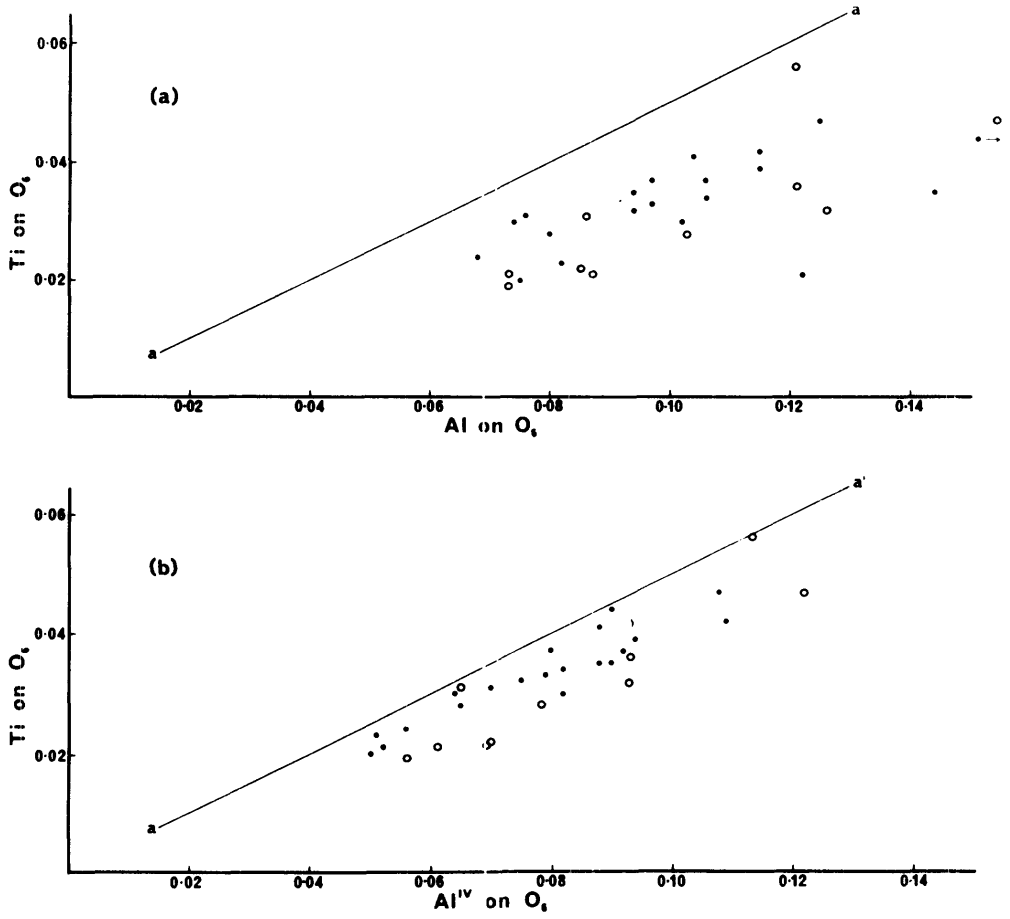

Fig. 5.5: Plots of Ti against Al^{total} (a) and Ti against Al^{IV} (b) for analysed pyroxenes from the low-Si series. The line aa' represents an Al:Ti ratio of 2:1. Open circles, pyroxene phenocrysts; filled circles, groundmass pyroxenes.

(iv) Crystallization of Pyroxenes in the Low-Si Series

The crystallization of pyroxenes from subalkaline mafic magma has received considerable attention in recent years and several detailed accounts are available of pyroxenes from tholeiitic intrusions (Brown, 1957; Brown and Vincent, 1963; McDougall, 1961; Atkins, 1969) and lavas (Muir and Tilley, 1964 ; Carmichael, 1967a; Evans and Moore, 1968; Nakamura and Kushiro, 1970a,b; Lowder, 1970).

The analysed pyroxenes of the low-Si series exhibit two features which are strongly at variance with accepted variation trends for pyroxenes from tholeiitic lavas. These are:

a) the absence of a Ca-poor pyroxene in the groundmass and of a reaction relation between olivine and liquid to produce Ca-poor pyroxene;

b) the increase in Ca content of the pyroxene with increasing Fe/Fe + Mg ratios (Fig. 5.3).

The presence of a Ca-poor pyroxene in the groundmass and (although less commonly observed) of a reaction relation between olivine and Ca-poor pyroxene (the Bowen-Anderson reaction) are widely cited as mineralogical evidence of tholeiitic affinities (MacDonald and Katsura, 1964; Tilley and Muir, 1967). However examination of approximately three hundred thin sections of rocks of the low-Si series has revealed no trace of either feature.

Considering the rather evolved nature of the lavas in question and their relatively high Fe/Mg ratios it is tempting to ascribe the absence of a Ca-poor pyroxene to passage of the liquids beyond the limit of the two pyroxene field whereby Ca-poor groundmass pyroxene disappears and its place

is taken by iron-rich olivine. Certainly this suggestion finds some support in the Fe-rich compositions of groundmass olivines of many lavas (Fo_{50-30}). However, compositional data on groundmass Ca-rich pyroxenes appear to lend little support to this proposal as a sole explanation. Firstly they are somewhat more magnesian than would be expected if they coexisted with a Ca-poor pyroxene near the limit of the two-pyroxene field. Tie lines joining Ca-rich and Ca-poor pyroxenes in Thingmuli lavas (Carmichael, 1967a) on the other hand, which suggest a more Fe-rich Ca-poor pyroxene than that produced by slow equilibrium cooling in the Skaerguard and Bushveld intrusions, may nullify this objection. Perhaps more importantly, the trend of increasing Ca contents with increasing Fe/Fe + Mg ratios suggests that at no stage during their crystallization were the Ca-rich pyroxenes tied to the pyroxene solvus, thereby precluding the crystallization of Ca-poor pyroxene at any stage.

Lindsley and Munoz (1969) have suggested that a_{SiO_2} may be an important control of the position of the two-pyroxene field boundary. As a natural corollary, when a_{SiO_2} falls to a sufficiently low value, the Bowen-Anderson reaction should cease to occur and groundmass Ca-poor pyroxene would in all likelihood be absent. More recently, Nicholls, Carmichael and co-workers have investigated in detail the effects of a_{SiO_2} on the stability of various natural assemblages in a wide variety of rock types and conditions (Carmichael *et al.*, 1970; Nicholls *et al.*, 1971; Nicholls and Carmichael, 1972; Bacon and Carmichael, 1973). Of particular interest to this discussion is the reaction:

$$Mg_2SiO_4 + SiO_2 = 2MgSiO_3 \qquad (1)$$

and its equilibrium relation

$$K = \frac{(a_{MgSiO_3})^2}{a_{SiO_2} \cdot a_{Mg_2SiO_4}}$$

from which it follows that an increase in a_{SiO_2} will stabilize $MgSiO_3$ relative to Mg_2SiO_4.

An estimate of a_{SiO_2} may be made using the reaction:

$$2Fe_3O_4 + 3SiO_2 = 3Fe_2SiO_4 + O_2. \qquad (2)$$

From equations derived by Nicholls and Carmichael (1972), a_{SiO_2} may be estimated providing values are available for $X^{Olivine}_{Fe_2SiO_4}$, $X^{Mt}_{Fe_3O_4}$, f_{O_2} and T under the quenching conditions. Unfortunately, ilmenite and magnetite rarely form a coexisting pair in the low-Si series and consequently a_{SiO_2} could only be calculated for the tholeiitic andesites 28050 and 28051. The latter is rather coarse grained and the quenching temperature and f_{O_2} (see Section 5.3, Table 5.4) appear somewhat low, suggesting some subsolidus re-equilibration. Consequently, the calculated value of $\log a^{liquid}_{SiO_2} = -0.800$ also appears rather low for a rock of this composition. On the other hand 28050 has undoubtedly been quenched rapidly, in fact so rapidly that pyroxene has not crystallized. It is likely that the calculated value of $\log a^{liquid}_{SiO_2} = -0.477$ represents a reasonable approximation for the remainder of the series.

Calculated values of a_{SiO_2} for 28050 and 28051 are plotted on Figure 5.6 (adapted from Carmichael *et al.*, 1970) together with lavas from Thingmuli, Lassen Peak and Talasea (Nicholls and Carmichael, 1972), Western Utah (data from Lowder, 1973) and Inverell, N.S.W. (data from N.T. Duggan, 1972), all of which contain a Ca-poor groundmass pyroxene but are similar

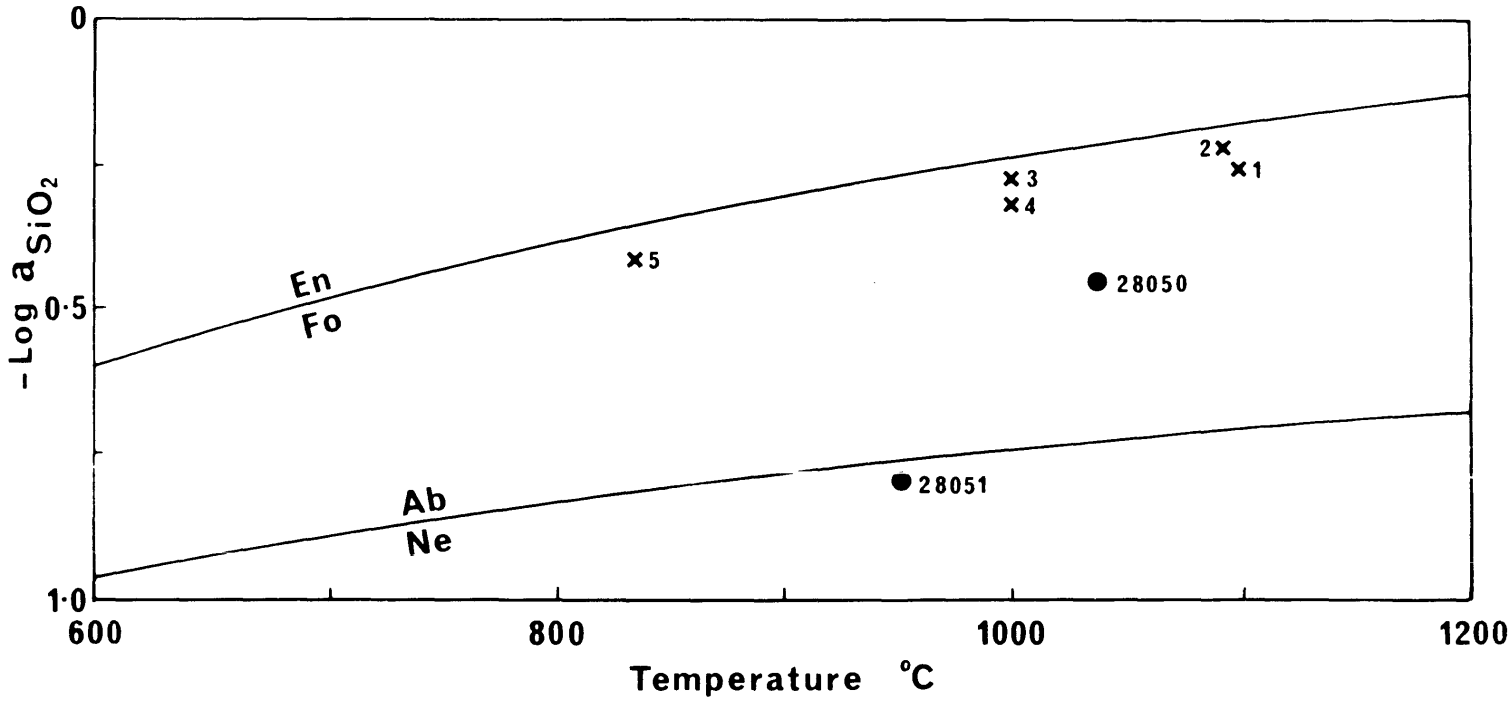

Fig. 5.6: Plot of silica activity (as log a SiO_2) against Fe-Ti oxide temperatures for two low-Si tholeiitic andesites (filled circles) and some representative rocks from other tholeiitic associations (crosses). Curves for the reactions En → Fo and Ab → Ne taken from Carmichael et al. (1970). 1, Thingmuli tholeiite (from Nicholls and Carmichael, 1972); 2, Inverell, N.S.W. tholeiite (data from Duggan, 1972); 3, Lassen Peak, U.S.A. andesite (from Nicholls and Carmichael, 1972); 4, Talasea, New Britain andesite (from Nicholls and Carmichael, 1972); 5, Western Utah basalt (data from Lowder, 1973).

to the rocks under discussion in terms of SiO_2 and qz contents. However they possess relatively lower $N_2O + K_2O$. While this data must be used with some caution it suggests that, despite similar levels of C.I.P.W. normative silica saturation (minor qz), silica activity has been significantly lower in the Tweed low-Si series during crystallization than in the other series. The relatively high Al and Ti contents of the pyroxenes accord with this conclusion (Gupta *et al.*, 1973).

The chemical factors governing silica activity in a silicate melt are extremely complex (Carmichael *et al.*, 1970) and it is therefore premature at this stage to suggest possible causes of this low a_{SiO_2}. From equation (2) above, it is evident that reduction of f_{O_2} will reduce a_{SiO_2}. Therefore the low values of a_{SiO_2} are a direct consequence of the low values of f_{O_2} determined for these rocks. Another explanation, consistent with the relatively high $Na_2O + K_2O$ of these rocks, is furnished by the data of Kushiro (1973). Kushiro demonstrated a shift of the forsterite-enstatite liquidus boundary in the system $MgO-SiO_2$ towards relatively more silica undersaturated compositions with addition of low valency elements, notably Na and K. Extrapolation of these results to natural compositions indicates that in lavas with similar silica saturation (in terms of qz), a high content of $Na_2O + K_2O$ should stabilize olivine relative to Ca-poor pyroxene as a phenocryst and groundmass phase i.e. the field of olivine is expanded relative to Ca-poor pyroxene in more undersaturated environments. Kushiro has, however, suggested an alternative explanation for the role played by $Na_2O + K_2O$, namely that high $Na_2O + K_2O$ supresses polymerization of SiO_4^{-4} tetrahedra in the melt so that the simple orthosilicate olivine structure would be favoured over

the more complex pyroxene chain silicate structure.

The somewhat aberrant increase in pyroxene Ca with increasing Fe/Fe + Mg in the low-Si series groundmass Ca-rich pyroxenes is also unique for rocks of these compositions. However, a similar trend has been observed in zoned pyroxenes in trachybasalts of southern California (Smith and Carmichael, 1969) and some lavas from southern Utah (Lowder, 1973); all the former and at least some of the latter are ne-normative. This particular trend was interpreted by Smith and Carmichael as a natural analogue to the trend in the system diopside-forsterite-silica (Kushiro and Schairer, 1963) where the Ca-rich pyroxene crystallizing from compositions close to the diopside-forsterite join becomes progressively enriched in the diopside component when the liquid pierces the diopside-forsterite join. This proposal does not seem relevant to the qz-normative liquids of the low-Si series.

Before discussing possible controls of this trend it should be noted that it is not necessarily strictly analogous to zoning. Within individual grains and indeed individual specimens, zoning appears to be absolutely minimal except in 28051 where a similar trend is evident from analyses of separate grains. In other specimens there are either insufficient analyses to confidently define a trend or the analyses show no significant variation in Ca, Mg, and Fe.

In the absence of a coexisting Ca-poor pyroxene, the groundmass Ca-rich pyroxenes were not necessarily tied to the two pyroxene solvus. The conventional crystallization trend away from the Di-Hd join and more or less directly toward the Fe apex in the pyroxene quadrilateral is usually

attributed to intersection of the pyroxene solidus by the solvus, the solvus shrinking progressively for more iron-rich compositions. Therefore if the composition were tied to the solvus then the trend could be explained simply by expansion of the solvus with falling temperatures (Boyd and Schairer, 1964). However, the more Ca and Fe-rich pyroxenes would appear to fall too close to the Di-Hd join to represent a simple expansion of the solvus. In addition, the augite phenocrysts in the iron-rich tholeiitic andesite 28056 do not fall significantly off the groundmass crystallization trend as might be expected with higher temperature intratelluric crystallization.

A more probable explanation for the trend involves the possible increase in oxygen fugacity with increasing whole rock Fe/Fe+Mg ratios throughout the series (see Section 5.3). Owing to the paucity of assemblages containing coexisting ilmenite and magnetitite, it has not been possible to obtain a quantitative expression of this increase. That it did occur, however, is strongly inferred by the change in the nature of the opaque oxide assemblage from ilmenite alone through ilmenite plus magnetite to magnetite alone. Figure 5.7 illustrates this changing assemblage in relation to pyroxene composition. It is suggested that increasing f_{O_2} has strongly suppressed the activity of Fe^{2+} relative to Fe^{3+} so that compositional variation has been governed dominantly by a Ca-Mg rather than a Fe-Mg substitution with increasing evolution of the host rocks. Throughout the series the relative Ca and Mg contents of the respective host rocks, indicating availability of these elements at the time of pyroxene precipitation, are consistent with this proposal.

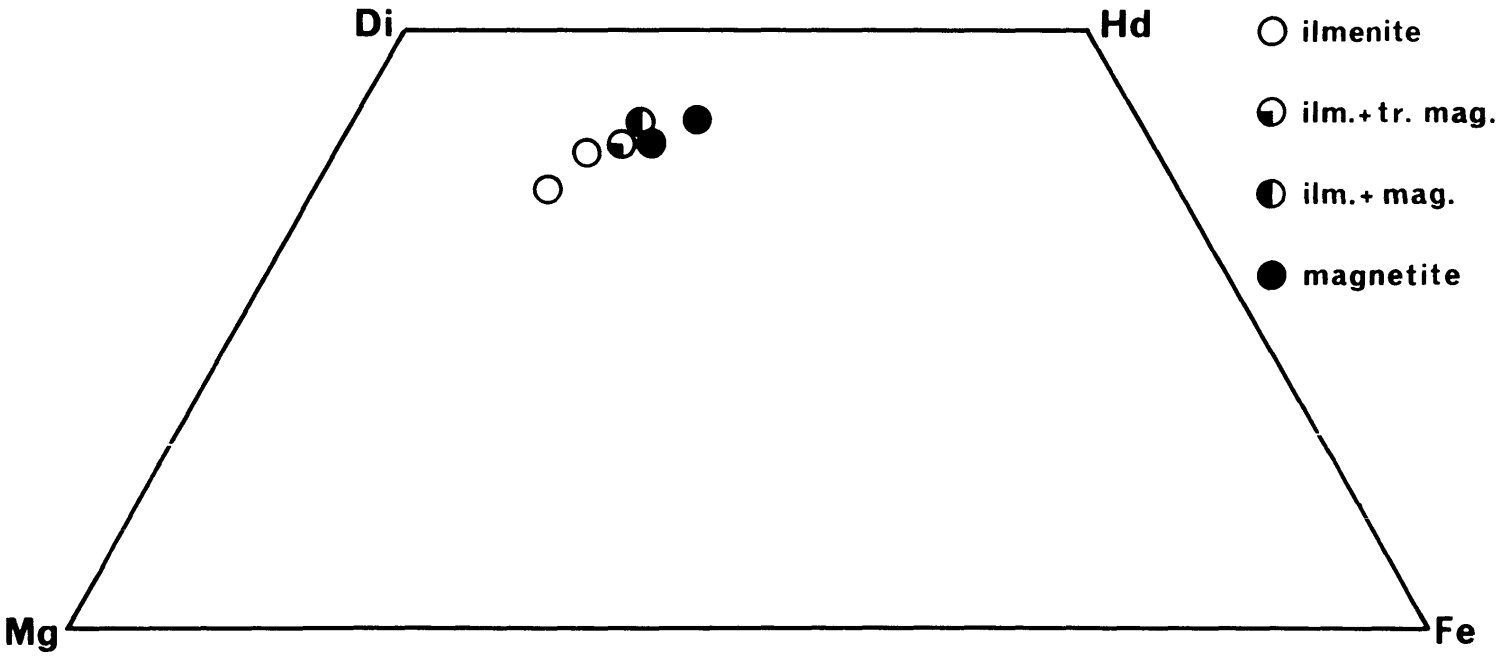

Fig. 5.7: The average compositions of pyroxenes from individual rocks of the low-Si series plotted in terms of Ca, Mg and Fe (atom %) in the conventional pyroxene quadrilateral in relation to the Fe-Ti oxide assemblage of their respective host rocks.

5.2.2 Pyroxenes of the High-Si Series

As noted above, rocks of the high-Si series usually contain augite and pigeonite as groundmass phases and many contain phenocrysts of augite, pigeonite and hypersthene.

Augite: Augite is a fairly common phenocryst in many of the tholeiitic andesites and icelandites of this series. Optical and textural data indicate two distinct generations of augite phenocrysts in many rocks. The first generation, a ferroaugite, consists of pale green to yellow-green phenocrysts up to 1 mm in diameter which are somewhat anhedral and usually show some evidence of resorption. They commonly occur in association with sieved and partially resorbed plagioclase phenocrysts of inferred high pressure origin and sometimes form intergrowths with plagioclase. Microprobe and optical data indicate that they are significantly enriched in Fe compared with the second generation of phenocrysts and groundmass grains. Subsequent reaction with the host liquid is indicated by marginal embayments and a spongey reaction structure somewhat reminiscent of that found in high pressure aluminian pyroxenes (Binns *et al.*, 1970). This structure pervades the whole crystal.

Second generation augites are small, elongate, colourless, primatic microphenocrysts less than 0.5 mm x 0.1 mm. They are usually euhedral, inclusion-free and occur as discrete microphenocrysts. They grade continuously in size to the Ca-rich pyroxene granules of the groundmass.

Pigeonite: Apart from their smaller optic axial angles pigeonite phenocrysts are difficult to distinguish optically from the second generation augites. The pigeonites are very pale yellow to colourless and

up to 0.5 mm in diameter. As far as could be ascertained, pigeonite phenocrysts are not mantled by augite. Similarly, groundmass pigeonite and augite are discrete phases with no mantling or zoning from one to the other.

Hypersthene: Hypersthene is restricted in occurrence to phenocrysts and microphenocrysts in tholeiitic andesites and icelandites. In some tholeiitic andesites (e.g. 28062) it can occur intergrown with (but always preceding) pigeonite and augite in aggregates of pyroxene and plagioclase. Discrete phenocrysts are stumpy prsimatic crystals up to 0.5 mm in diameter and are invariably enveloped by a thin mantle of pigeonite. The orthopyroxene exhibits very faint pleochroism with X = very pale pink; Z = very pale green.

Orthopyroxene phenocrysts occurring in rhyolitic pitchstones are strongly enriched in Fe and are distinctly pleochroic with X = yellow brown; Z = pale green. These ferrohypersthenes commonly occur in close association with microphenocrysts of ilmenite which may also form abundant small inclusions. There is no evidence of incongruent breakdown of orthopyroxene to produce fayalitic olivine as a by-product.

(i) Compositional Data

Electron microprobe data on pyroxenes from twelve rocks of the high-Si series are listed in Table II.2b (Appendix II). Selected analyses and some average analyses are set down in Table 5.2 to illustrate principal chemical features and compositional trends among pyroxenes of this series.

Compositional relations among the pyroxenes in terms of Ca, Mg and Fe for rocks of the high-Si series are illustrated in Figure 5.8 and for

TABLE 5.2

SELECTED MICROPROBE ANALYSES OF PYROXENES FROM MEMBERS OF THE HIGH-Si SERIES AND A RHYOLITIC PITCHSTONE

	1	2	3	4	5	6	7	8	9
SiO_2	49.50	49.84	51.62	51.93	52.03	51.21	51.98	50.77	48.57
TiO_2	0.61	0.31	0.84	0.85	0.38	0.33	0.45	0.17	0.25
Al_2O_3	1.33	1.03	3.31	1.85	1.02	1.01	1.28	1.34	0.78
FeO	22.18	24.23	7.95	13.56	23.43	25.40	22.06	32.45	38.35
MnO	0.55	0.69	-	0.22	0.51	0.52	0.33	0.68	0.80
MgO	7.36	7.39	15.60	14.28	18.38	17.53	21.42	15.00	9.98
CaO	18.35	16.78	19.80	17.80	4.25	3.37	2.02	0.45	1.07
Na_2O	-	0.15	0.59	0.25	0.20	-	-	-	-
Total	99.90	100.42	99.71	100.95	100.20	99.37	99.54	100.86	99.80
Si	1.955	1.968	1.912	1.941	1.968	1.968	1.953	1.969	1.973
Al^{IV}	0.045	0.032	0.088	0.059	0.032	0.032	0.047	0.031	0.027
Al^{VI}	0.017	0.016	0.056	0.022	0.013	0.014	0.010	0.030	0.010
Ti	0.018	0.009	0.023	0.024	0.011	0.010	0.013	0.005	0.008
Fe	0.733	0.800	0.246	0.424	0.741	0.816	0.693	1.052	1.303
Mn	0.019	0.023	-	0.007	0.016	0.017	0.011	0.022	0.028
Mg	0.433	0.435	0.861	0.795	1.036	1.004	1.199	0.867	0.604
Ca	0.776	0.710	0.786	0.713	0.172	0.139	0.081	0.019	0.047
Na	-	0.011	0.042	0.018	0.015	-	-	-	-
Σ xy	2.00	2.00	2.01	2.00	2.00	2.00	2.01	2.00	2.00
Atom%									
Ca	40.0	36.5	41.5	36.9	8.8	7.1	4.1	1.0	2.4
Mg	22.3	22.4	45.5	41.2	53.2	51.2	60.8	44.7	30.9
Fe	37.7	41.1	13.0	21.9	38.0	41.7	35.1	59.3	66.7
100 Fe/Fe+Mg	62.8	64.7	22.2	34.7	41.7	44.9	36.6	54.8	68.3

KEY TO TABLE 5.2

1. Ferroaugite phenocryst in high-Si tholeiitic andesite 28061 (Table II.2b, Anal. 10).

2. Ferroaugite phenocryst in icelandite 28072 (Table II.2b, Anal. 96).

3. Augite in high-Si tholeiitic andesite 28065 (Table II.2b, Anal.45).

4. Augite phenocryst in high-Si tholeiitic andesite 28062 (Table II.2b, Anal. 31).

5. Pigeonite phenocryst in high-Si tholeiitic andesite 28062 (Table II.2b, Anal. 27).

6. Pigeonite phenocryst in high-Si tholeiitic andesite 28061 (Table II.2b, Anal. 5).

7. Hypersthene phenocryst in high-Si tholeiitic andesite 28062 (Table II.2b, Anal. 17).

8. Hypersthene phenocryst in rhyodacite 28073 (Table II.2b, Anal. 101).

9. Ferrohypersthene phenocryst in rhyolitic pitchstone 28076 (Table II.2c, Anal. 11).

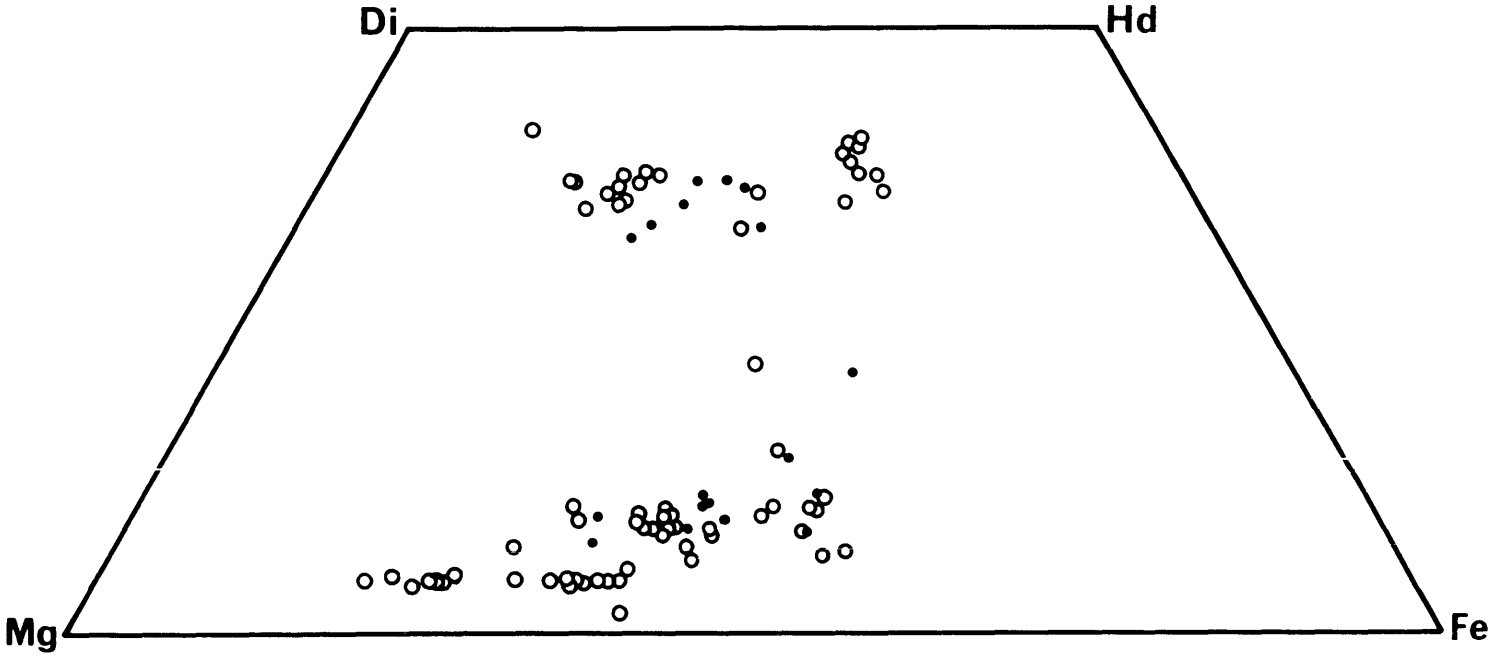

Fig. 5.8: Collation of microprobe data on pyroxenes from members of the high-Si series and the rhyolites plotted in terms of Ca, Mg and Fe (atom %) in the conventional pyroxene quadrilateral. Open circles, pyroxene phenocrysts; filled circles, groundmass pyroxenes.

individual rocks in Figure 5.9. The complex variation within and between pyroxenes from various extrusives is immediately obvious.

With the exception of one phenocryst and one groundmass pyroxene from icelandite 28067 there is a well defined miscibility gap between the Ca-rich and Ca-poor pyroxenes. The presence of a miscibility gap between coexisting low pressure pyroxenes in tholeiitic lavas has been widely recognized (Carmichael, 1967a; Evans and Moore, 1968; Schorer, 1970), and is supported by the present data.

A wide variation in Fe/Fe+Mg ratios is apparent for all three pyroxene species. The compositions of the ferroaugite phenocrysts are confined to a relatively compact area within the quadilateral and they more or less coincide with that part of the Skaergaard pyroxene trend where Ca increases after the liquid has passed beyond the limit of the two-pyroxene field, a more Fe-rich olivine now reappearing. It is perhaps significant that these Fe-rich augites only occur in Tweed lavas with high Fe/Fe+Mg ratios and in which olivine (usually Fe-rich) has been an early crystallizing phenocrysts phase.

While showing some scatter in terms of Ca content, the second generation augites also broadly coincide with the Skaergaard Ca-rich pyroxene trend in the range $Ca_{40}Mg_{45}Fe_{15}$ to $Ca_{35}Mg_{30}Fe_{25}$.

Pigeonite phenocrysts vary slightly in Ca content within and between different lavas. The pigeonite 100 Fe/Fe+Mg ratios vary from 35 to 58 and to some extent are dependent on the Fe/Fe+Mg ratio of the host rock. Within an individual host the Fe/Fe+Mg ratio of the pigeonite is generally higher than this ratio for the coexisting hypersthene; however there is an

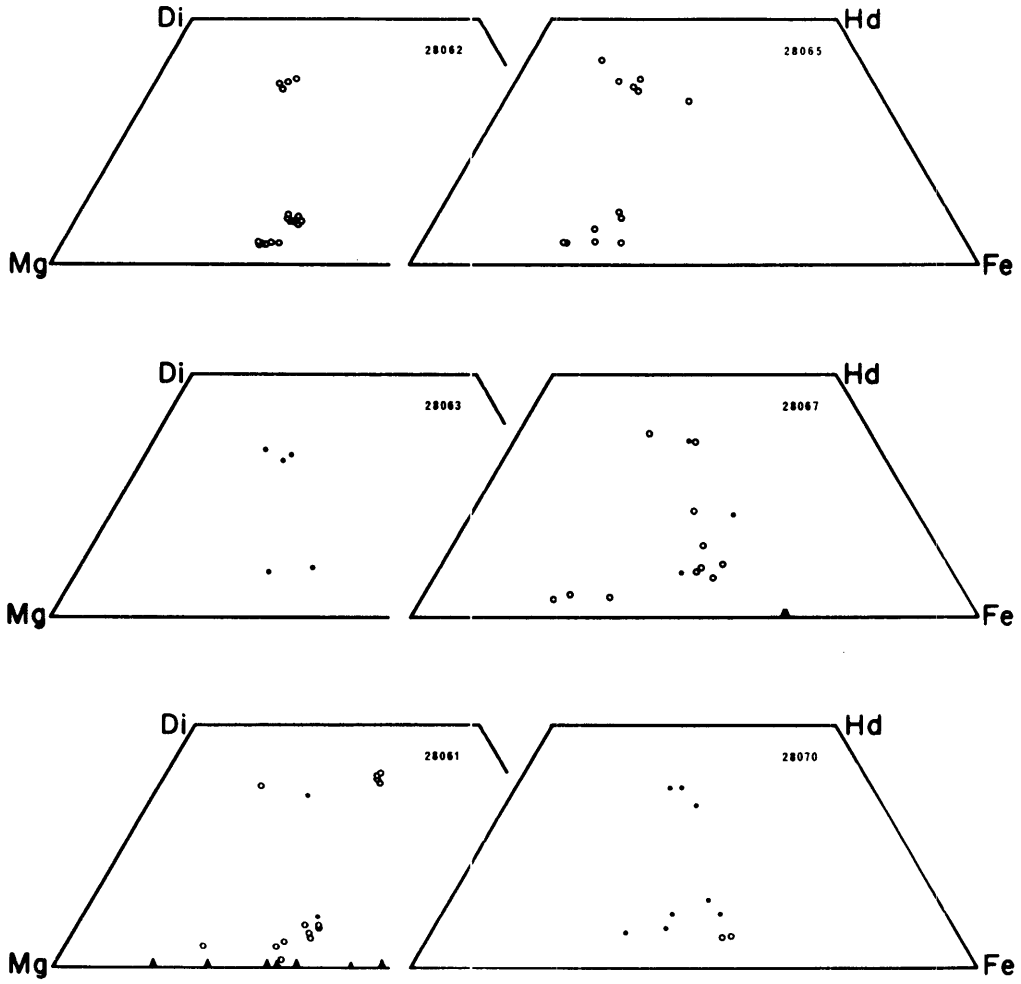

Fig. 5.9: Analysed pyroxenes and olivines from individual rocks of the high-Si series and rhyolites plotted in terms of Ca, Mg and Fe (atom %) in the conventional pyroxene quadrilateral. Open circles, pyroxene phenocrysts; filled circles, groundmass pyroxenes; large triangles, olivine phenocrysts; small triangles, groundmass olivines.

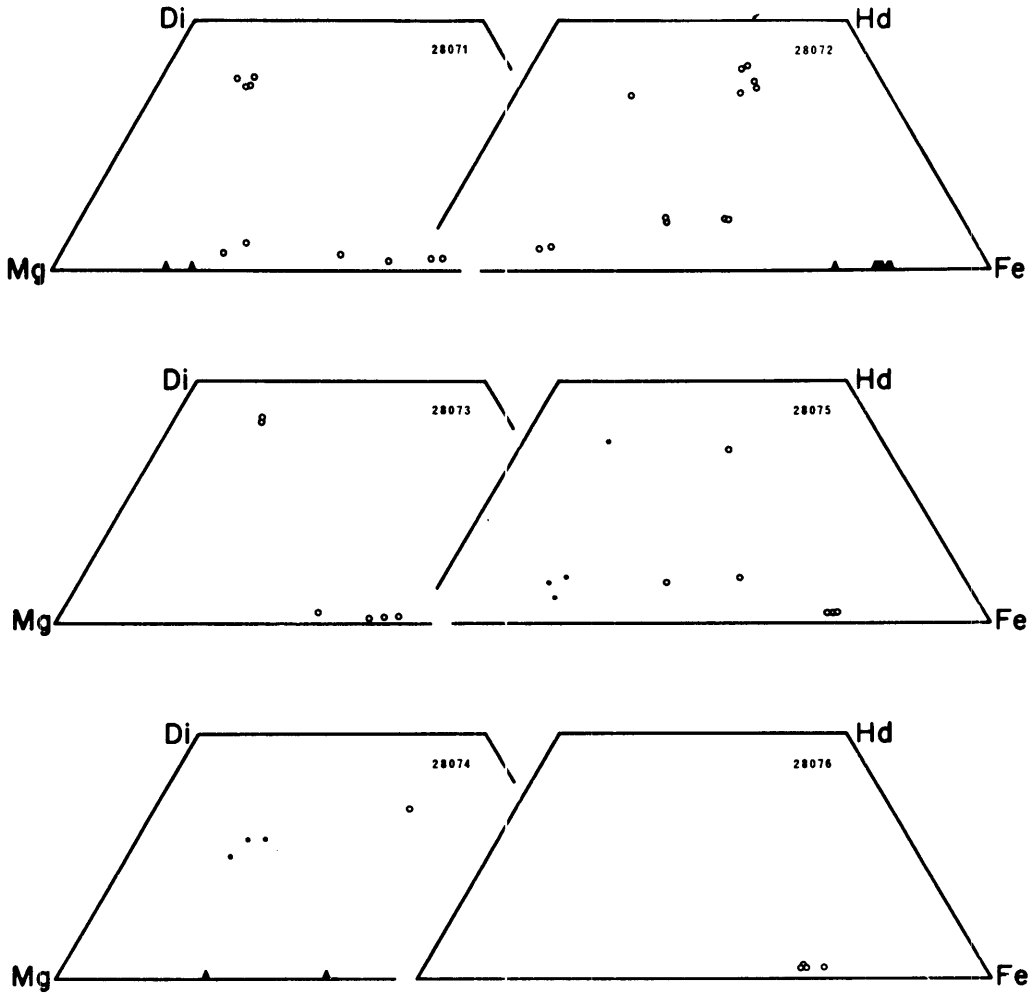

Fig. 5.9 (Continued).

overlap in overall variation (Fig. 5.8).

The Ca content of the pigeonite phenocrysts does not vary systematically with increasing Fe/Fe+Mg ratio. The relatively few analyses of groundmass pigeonites suggest that Ca rises systematically with increasing Fe/Fe+Mg ratios and accords with similar data on pigeonite-bearing lavas (e.g. Carmichael, 1967a; Schorer, 1970). In the Makaopuhi tholeiitic lava lake in Hawaii, rapid chilling in the upper portions of the lake produces a pronounced increase in pigeonite Ca content with increasing Fe/Fe+Mg whereas in the more slowly cooled central positions, Ca remains essentially constant (Evans and Moore, 1968). A more or less constant Ca content also characterises pigeonites and inverted pigeonites from large slowly cooled tholeiitic intrusions (Brown, 1957,1967; Atkins, 1969), thereby defining the crystallization of pigeonite under equilibrium conditions.

Orthopyroxene phenocrysts in tholeiitic andesite and icelandite are relatively magnesian with 100 Fe/Fe+Mg ratios in the range 20-40. Ca is relatively constant at about 4 mol %. However the Fe/Fe+Mg ratio is not necessarily dependent upon that of the host rock and in fact the most magnesian orthopyroxenes (100 Fe/Fe+Mg ~20) occur in an evolved icelandite (28072) with 100 Fe/Fe+Mg = 78.

Partitioning of the minor elements Ti, Al, Mn and Na between coexisting Ca-rich and Ca-poor pyroxenes follows well established patterns. Al, Ti and Na are preferentially incorporated in augite relative to pigeonite and hypersthene and Mn is enriched in the latter.

Figures 5.10a and 5.10b illustrate the relationship between Ti and Al^{total} and Ti and Al^{IV} in the three pyroxene species. The close relationship

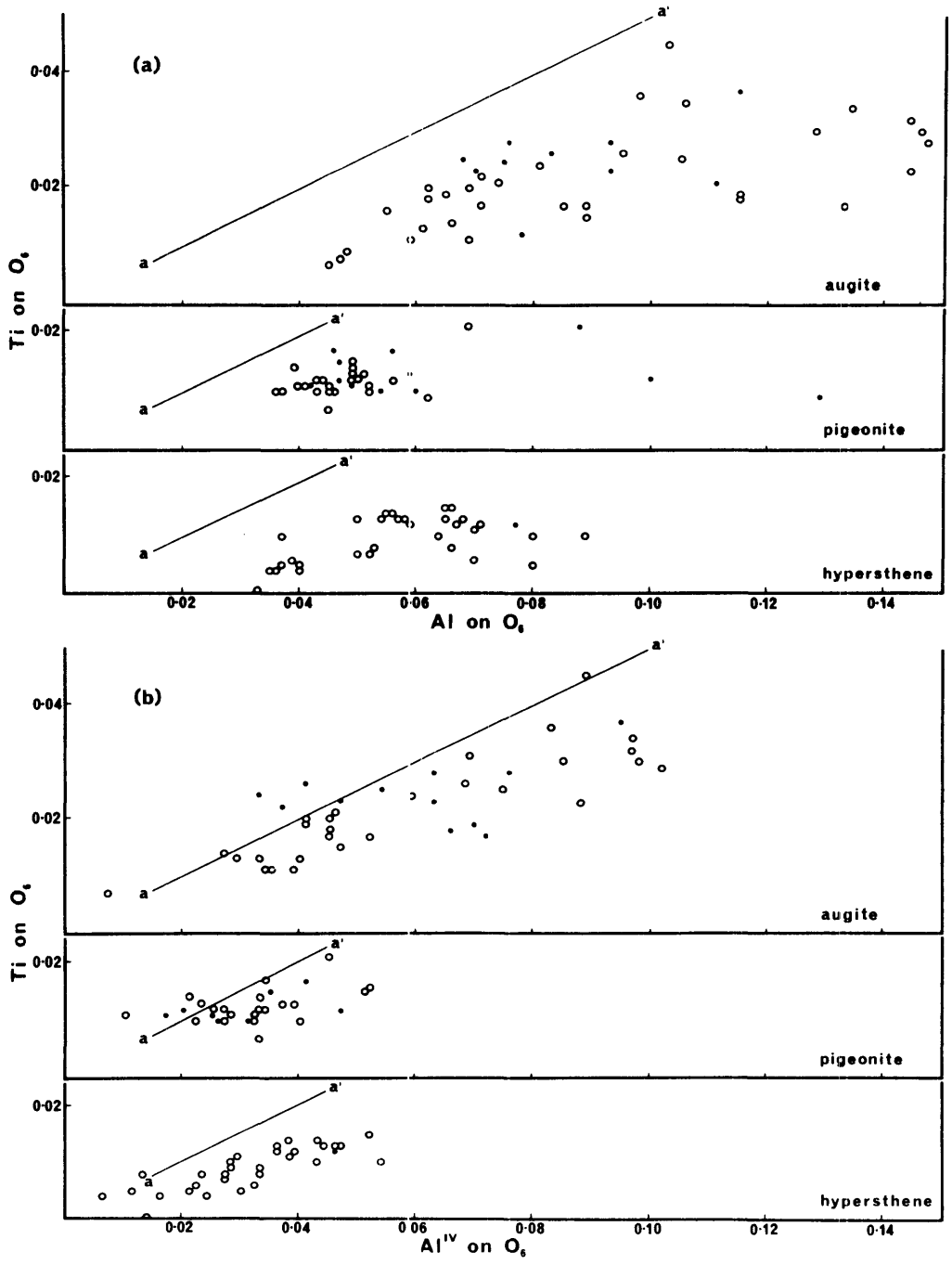

Fig. 5.10: Plots of Ti against Al^{total} (a) and Ti against Al^{IV} (b) for analysed pyroxenes from rocks of the high-Si series and rhyolites. The line aa' represents an Al:Ti ratio of 2:1. Open circles, pyroxene phenocrysts; filled circles, groundmass pyroxenes.

between Ti and Al^{IV}, particularly in augite and hypersthene, is clearly evident. Substitution of Al and Ti in the pyroxene structure is usually ascribed to entry of the so-called "titanpyroxene" component $CaTiAl_2O_6$ (Yagi and Onuma, 1967). Ideally this type of substitution should produce an Al^{IV}/Ti ratio of 2. Almost all analysed pyroxenes display higher ratios, thereby suggesting that minor Ca and Fe^{3+} have entered the structure in sixfold co-ordination coupled with Al^{IV} (e.g. as $CaFe^{3+}(AlSi)O_6$.

Control of the degree of substitution at low pressures of a titanopyroxene "component" in augite is customarily assigned to the availability of Si in the host melt (Kushiro, 1960; Le Bas, 1962). Recently Gupta *et al.* (1973) have demonstrated this experimentally in the system $CaMgSi_2O_6$-$CaTiAl_2O_6$-SiO_2. They showed that the $CaTiAl_2O_6$ content of diopside falls steadily with increasing silica saturation of the melt until virtually pure $CaMgSi_2O_6$ forms in silica-saturated compositions where tridymite is a co-existing phase. Strong evidence in support of this data is provided by Figure 5.11 which illustrates the close correlation between pyroxene Al-Si substitution and qz of the respective host rocks. Si-Al relations in groundmass augite are less well defined, probably reflecting non-equilibrium conditions during quenching.

The ferrohypersthene phenocrysts of the rhyolitic pitchstones are rather unique in composition. Their composition relative to the so-called "forbidden" zone of Smith (1972) is shown in Figure 5.12. Within this zone Fe-rich Ca-poor pyroxenes are unstable relative to the assemblage Fa-rich olivine plus quartz at 925°C, which is probably close to the actual eruptive temperatures of the rhyolitic pitchstones. The stability of these pyroxenes

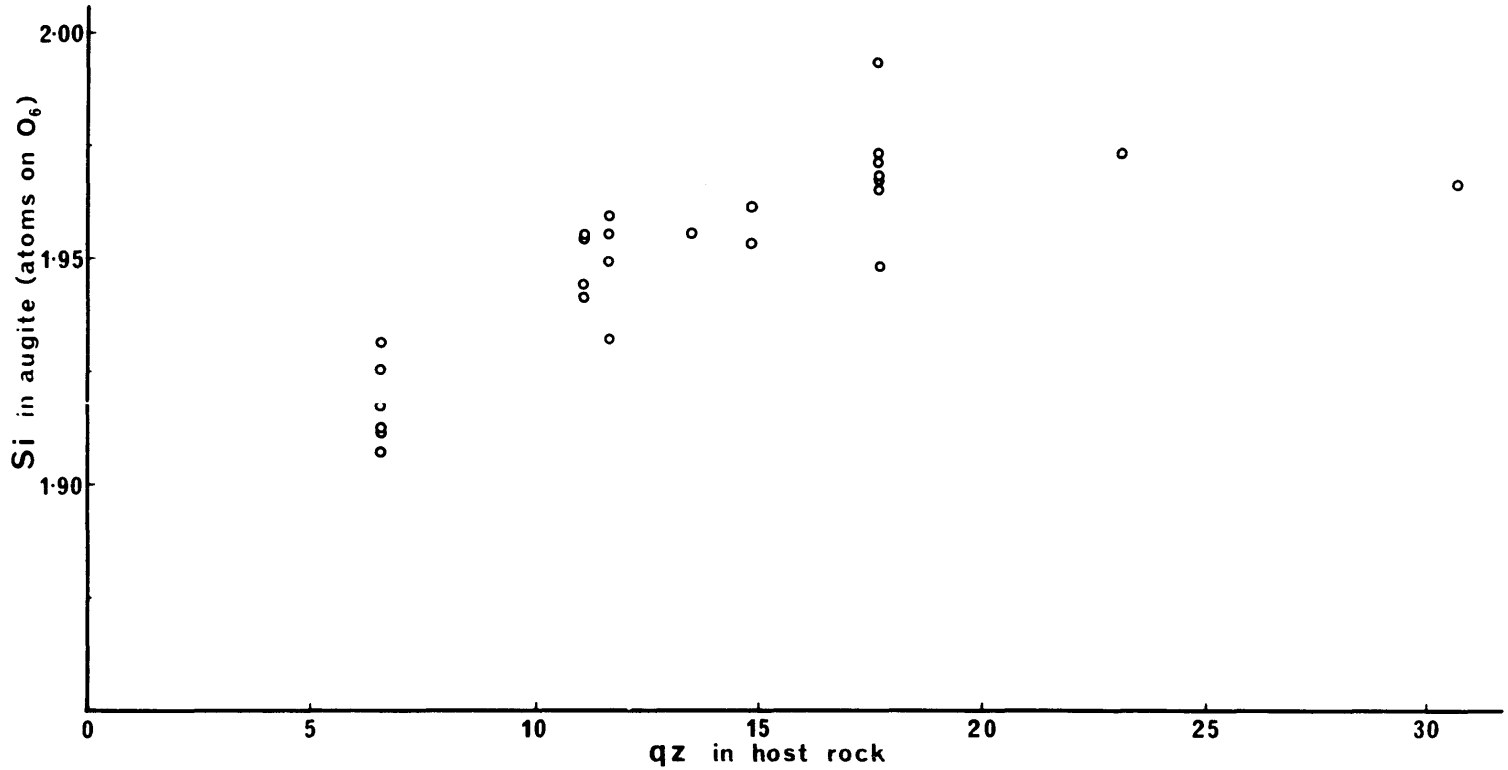

Fig. 5.11: Diagram illustrating the relationship between the Si contents of pyroxene phenocrysts (atoms on the basis of 6 oxygen atoms) from rocks of the high-Si series and rhyolites and the normative qz contents (wt %) of their respective host rocks.

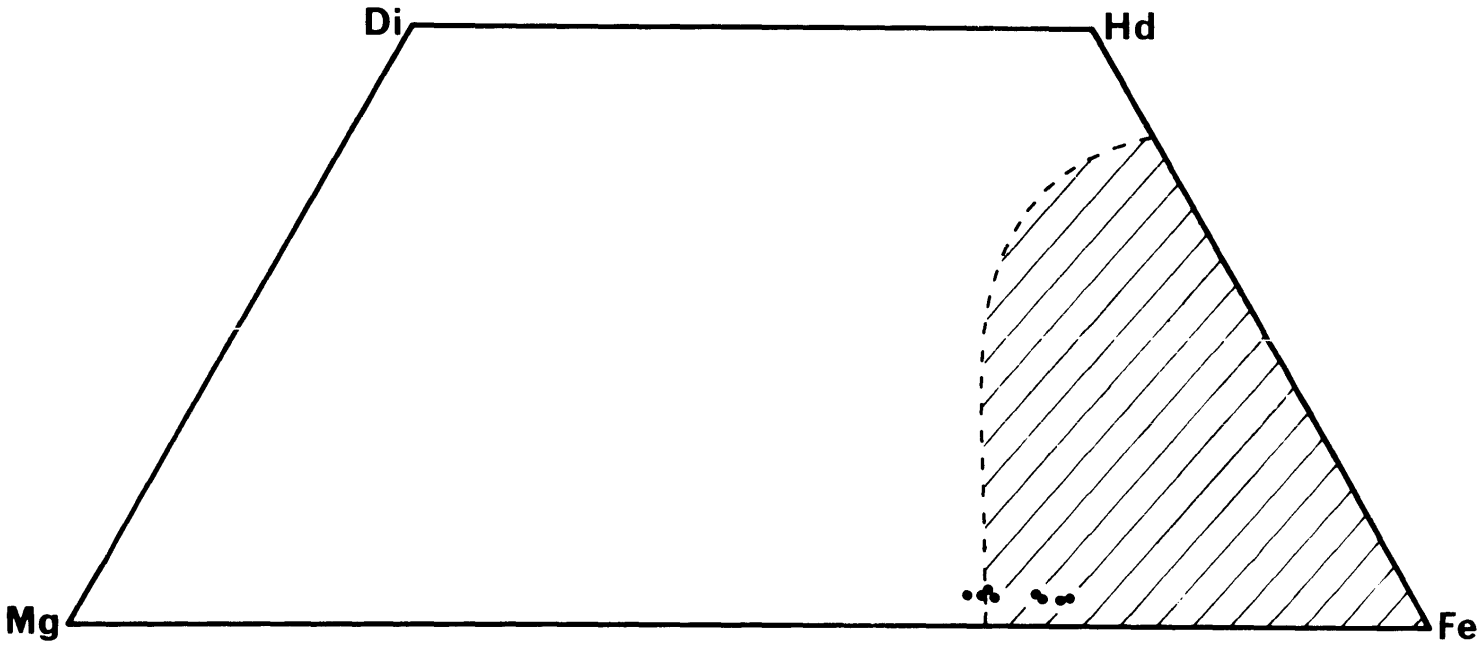

Fig. 5.12: Ferrohypersthene phenocrysts from rhyolitic pitchstones plotted in terms of Ca, Mg and Fe (atom %) in the conventional pyroxene quadrilateral and their relationship to the "forbidden zone" of iron rich pyroxenes at 925°C and 1 atmosphere (Smith, 1972).

will be discussed in the following section. Hypersthene phenocrysts in a tholeiitic rhyodacite 28073 are intermediate in composition between the two generalised groups discussed above. They are notably poor in Ca (2 mol %) and low in Ti and Al. Their Ca-poor nature probably reflects, at least in part, the Ca-poor nature of the host rock which contains a trace of normative corundum.

(ii) Pyroxene Crystallization in the High-Si Series

Compositional and textural relationships among the ferromagnesian minerals in the high-Si series suggest a complex crystallization history. Generalized trends illustrated in Figure 5.13 indicate the likely crystallization sequence. The early separation of ferroaugite (with or without coexisting olivine) in some rocks, followed by Mg-rich augite, pigeonite and hypersthene, should be particularly noted. However it must be emphasised that the trends portrayed in Figure 5.13 are highly generalized and all steps need not necessarily be present.

Compositional trends for pyroxenes in rocks lacking early ferroaugite closely parallel well established trends for other intrusive and extrusive tholeiitic associations, e.g. Skaergaard (Brown, 1957; Brown and Vincent, 1963), Red Hill, Tasmania (McDougall, 1961), Thingmuli, Iceland (Carmichael, 1967), Makaopuhi lava lake, Hawaii (Evans and Moore, 1968) and Bushveld (Atkins, 1969). However, early crystallization of ferroaugite in many Tweed rocks followed by more magnesian Ca-rich and Ca-poor pyroxenes is at variance with the normal trend for pyroxenes in subalkaline magmas. The ferroaugites coexist with and are sometimes intergrown with sieved plagioclase which has apparently crystallized at elevated pressures under

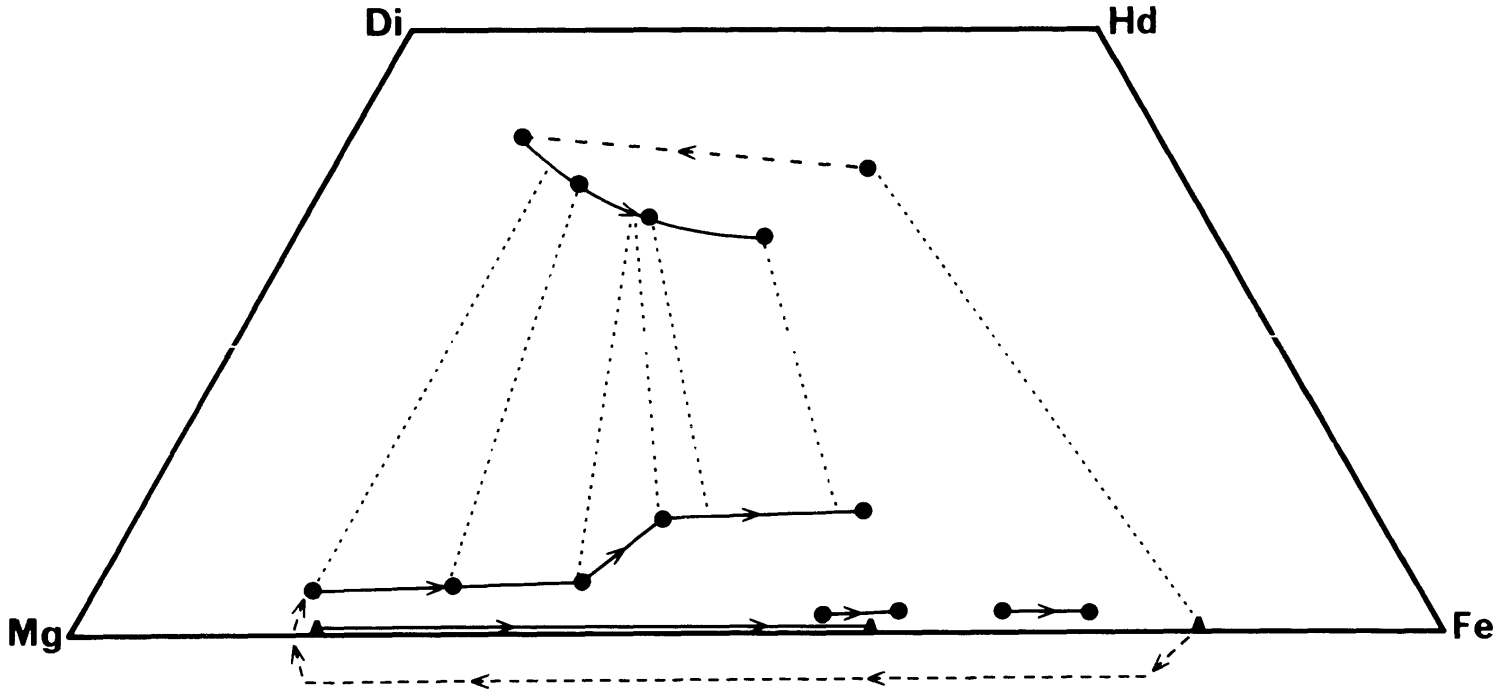

Fig. 5.13: Generalized trends of olivine and pyroxene crystallization in rocks of the high-Si series and the rhyolites.

exceptionally low f_{O_2} and P_{H_2O} (discussed in Section 5.4). Low f_{O_2}, probably broadly equivalent to or slightly above the wüstite-magnetite buffer, would be especially favourable to entry of Fe^{2+} into the pyroxene structure (see following discussion). The ferroaugites and their coexisting olivines are not dissimilar in composition to analagous phenocrysts in some Thingmuli andesites. However a second generation of augite phenocrysts is absent from the Thingmuli andesites and very fine grainsize precluded microprobe analysis of groundmass augite by Carmichael (1967a).

The rather dramatic effect of unusually high f_{O_2} on Fe/Fe+Mg ratios of olivine and pyroxene is amply demonstrated by the Fe^{3+}-rich Kolbiensey Basalt north of Iceland (Sigurdsson and Brown, 1970), which contains almost pure forsterite ($Fo_{98.8}$), enstatite ($Ca_4Mg_{88}Fe_8$) and highly magnesian augite (average $Ca_{39}Mg_{51}Fe_{10}$).

Quantitative data on the effect of varying f_{O_2} on entry of Fe^{2+} into ferromagnesian minerals in natural rock compositions are not presently available. Several authors have studied crystallization under controlled f_{O_2} conditions (Holloway and Burnham, 1971; Helz, 1973; Thompson, 1973) but only very limited compositional data have been published on the crystallizing phases. In the absence of this data a short discussion is warranted on a few simple thermodynamic considerations which illustrate the likely effect of f_{O_2} on the Fe/Fe+Mg ratios of the ferromagnesian phases.

Entry of Fe^{2+} into the pyroxene structure is dependent upon the activity of $FeSiO_3$ in the pyroxene ($a^{Px}_{FeSiO_3}$). Consider the equation:

$$FeSiO_3 = FeO + SiO_2$$

for which $\log a^{Px}_{FeSiO_3} = \frac{\Delta Go}{2.303RT} + \log a^{liquid}_{FeO} + \log a^{liquid}_{SiO_2}$

At constant $a^{liquid}_{SiO_2}$, an increase in a^{liquid}_{FeO} will increase $a^{Px}_{FeSiO_3}$.

Now considering the equations:

$$1/3\ Fe_3O_4 = FeO + 1/6\ O_2$$

and

$$FeO = Fe + \tfrac{1}{2}O_2$$

for which $\log a^{liquid}_{FeO} = \frac{\Delta Go}{2.303RT} + 1/3 \log a^{Mt}_{Fe_3O_4} - 1/6 \log f_{O_2}$

and $\log a^{liquid}_{FeO} = \frac{\Delta Go}{2.303RT} + \log a^{iron}_{Fe} + \tfrac{1}{2}f_{O_2}$.

It follows that a value of f_{O_2} will exist for which a^{liquid}_{FeO} (and thus $a^{Px}_{FeSiO_3}$) will be a maximum for a given T, P and Fe content of the liquid. This value for f_{O_2} should fall within limits defined by the wüstite-magnetite and iron-wüstite buffers which are controlled by the above reactions.

Second generation pyroxene microphenocrysts represent a considerably later low pressure crystallization episode. They are always small and euhedral and display no evidence of resorption. Ilmenite phenocrysts preceded the crystallization of these pyroxene microphenocrysts and this has undoubtedly lowered the Fe/Fe+Mg ratios of the host liquids since the shift in Fe/Fe+Mg ratios of the pyroxenes to more Mg-rich compositions is greatest in rocks with low FeO and MgO (e.g. the evolved icelandite, 28072; FeO = 4.13%, MgO = 0.77%). However the amount of ilmenite in the rock appears to be too low (<1%) for this order of crystallization to be the sole cause of the shift to more magnesian pyroxene compositions. An additional control in the light

of the above discussion may be a significant rise in f_{O_2} prior to their precipitation causing a reduction in a^{liquid}_{FeO} (and therefore $a^{Px}_{FeSiO_3}$). A rise in f_{O_2} in water-deficient low f_{O_2} magmas is not unexpected with ascent to near surface conditions where the liquid may gain some water from surrounding country rocks.

In members of the high-Si series lacking ferroaugite, coexisting sieved plagioclases are rare and, where present, are very extensively resorbed. It is likely therefore that extended periods under low pressure intratelluric conditions have resulted in complete resorption of early formed ferroaugite.

iii) Hypersthene-Pigeonite Relations

Relationships between hypersthene and pigeonite in many intermediate tholeiitic rocks have received considerable attention from petrologists. With progressive iron enrichment the assemblage changes from augite-hypersthene to augite-pigeonite (Hess, 1941; Brown and Vincent, 1963; Brown, 1967); the intermediate three phase assemblage augite-pigeonite-hypersthene is not uncommon (Kuno, 1950; Muir, 1954; Isshiki, 1963; Nakamura and Kushiro, 1970a,b).

Hess (1941) suggested that with progressive cooling and iron enrichment in a magma the cooling curve crossed a more steeply inclined orthorhombic-monoclinic inversion curve (Fig. 5.14a). He based this proposal on the rhombic enstatite-clinoenstatite inversion on the join $MgSiO_3$-$FeSiO_3$ determined by Bowen and Schairer (1935). However it has been subsequently shown that in the Mg-rich portion of the system $MgSiO_3$-$FeSiO_3$ protoenstatite rather than clinoenstatite is the stable high temperature phase, protoenstatite

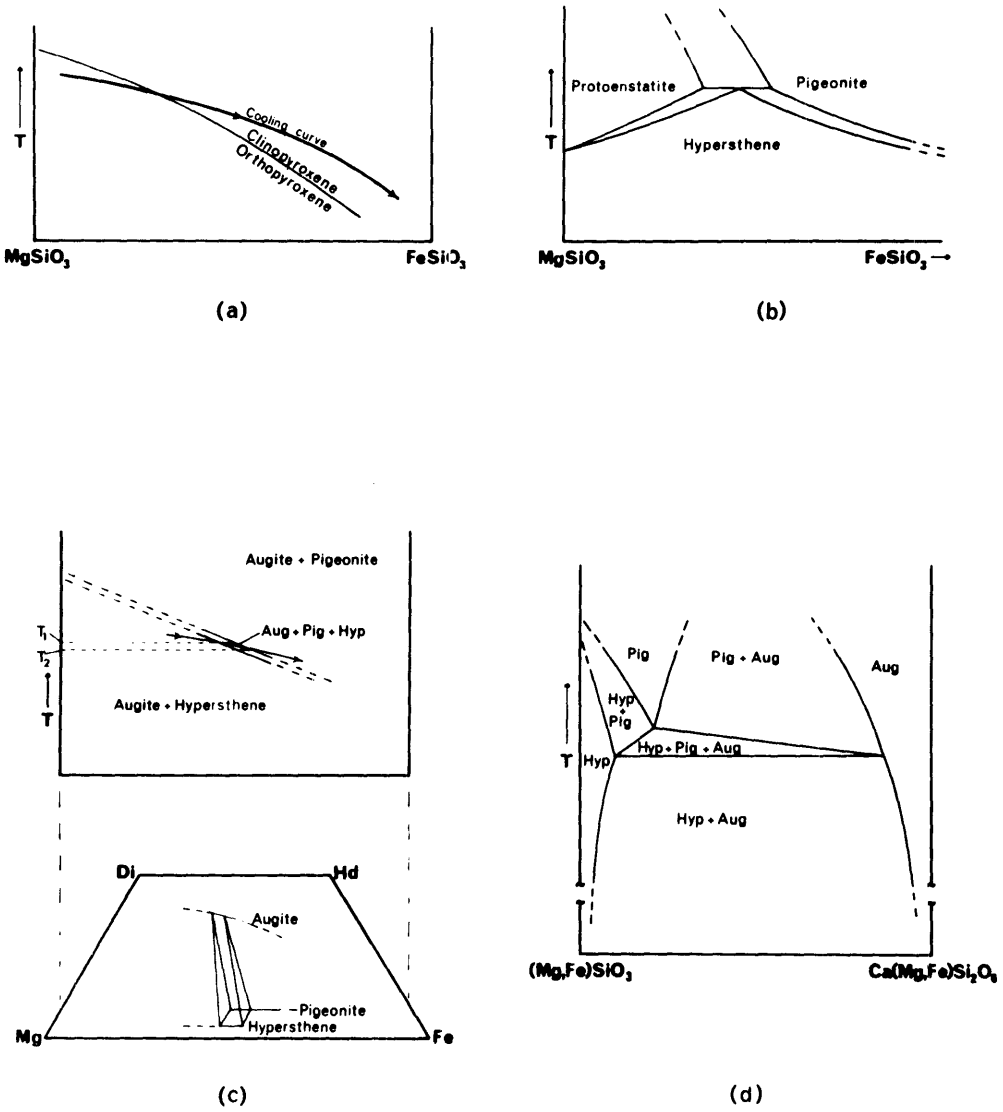

Fig. 5.14: Various interpretations of the relationships between hypersthene and pigeonite. (a) After Hess (1941). (b) After Boyd and Schairer (1964). (c) After Nakamura and Kushiro (1970). (d) After Virgo and Ross (1973). See text for discussion.

inverting to clinoenstatite on cooling (Foster, 1951; Atlas, 1952). Boyd and Schairer (1964) suggested a relationship between protoenstatite, hypersthene and pigeonite of the type shown in Figure 5.14b and this interpretation was further developed by Kuno (1966). A major criticism of both the above models is their failure to consider pigeonite as a Ca-bearing mineral and therefore to take account of the role of Ca in the stability of pigeonite. Nakamura and Kushiro (1970b) have suggested that with increasing iron enrichment pigeonite forms at the expense of hypersthene through a reaction

$$\text{hypersthene} + \text{liquid} \rightleftarrows \text{pigeonite}$$

where the host liquid must be more Ca and Fe rich than the Ca-poor pyroxene phases involved. This is illustrated schematically in Figure 5.14c. On the other hand Virgo and Ross (1973) have described coexisting orthopyroxene ($Ca_2Mg_{45}Fe_{53}$) and pigeonite ($Ca_4Mg_{42}Fe_{54}$) in a Mull andesite (inninmorite; Bailey *et al.*, 1924) and offer yet another interpretation of the orthopyroxene-pigeonite relationship which is illustrated schematically in Figure 5.14d. They contend that the Mull inninmorite pyroxene assemblage orthopyroxene-pigeonite represents a quench across the narrow inversion interval orthopyroxene-low-Ca pigeonite at a higher temperature relative to the three phase assemblate orthopyroxene ($Ca_4Mg_{54}Fe_{42}$-$Ca_4Mg_{47}Fe_{49}$)-pigeonite ($Ca_8Mg_{48}Fe_{44}$-$Ca_9Mg_{35}Fe_{56}$)-(augite $Ca_{38}Mg_{37}Fe_{25}$-$Ca_{35}Mg_{29}Fe_{36}$) of the Weiselberg andesite described by Nakamura and Kushiro (1970b). It is difficult to reconcile the subsolidus relationships illustrated in Figure 5.14d with experimental data on the join $MgSiO_3$-$CaMgSi_2O_6$ (Boyd and Schairer, 1964) which show that at subsolidus temperatures the pyroxene solvus shrinks with increasing temperature

and therefore Ca-poor pyroxenes are actually enriched in Ca. It seems unlikely that this relationship will be fundamentally different in the Fe-bearing portion of the pyroxene quadrilateral. Therefore one would expect the field orthopyroxene + pigeonite to be actually displaced at higher temperatures to more Ca-rich compositions rather than toward the $MgSiO_3$-$FeSiO_3$ join.

In the Tweed high-Si series, augite, pigeonite and hypersthene commonly occur in the same rock. Unfortunately, in view of the wide variation in Fe/Fe+Mg ratios commonly observed in the hypersthenes and pigeonites (Figs. 5.8, 5.9) it seems likely that the pyroxenes crystallized over a wide temperature interval. However in one tholeiitic andesite (28062) the pyroxenes show little variation in composition (Fig. 5.8) and hence one may assume that they crystallized over a relatively limited temperature interval. In this rock (and other closely similar examples) orthopyroxene is always mantled by pigeonite. Furthermore, the interface between the pigeonite and orthopyroxene is invariably highly irregular (see Plate 4, No.6), the orthopyroxene being strongly embayed and the pigeonite sometimes occurring as a granular aggregate. These relations strongly support the model of Nakamura and Kushiro (1970). Thus with progressive pyroxene crystallization and increase in Fe/Fe+Mg ratio of the residual liquid, pigeonite appears in place of orthopyroxene and earlier orthopyroxene reacts with the liquid to produce a mantle of pigeonite. In particular, the granular nature of many of the pigeonite mantles are strongly at variance with the alternative models which require either that the orthopyroxene and pigeonite coexist as an equilibrium assemblage (Virgo and

Ross, 1973) or that an inversion from the orthorhombic to the monoclinic phase occurs with iron-enrichment and/or falling temperature. Nevertheless it must be emphasized that inversion of pigeonite to orthopyroxene with falling temperature, and the attendant exsolution of lamellae of Ca-rich pyroxene (Hess, 1941; Brown, 1967), is of course important in large slowly cooled tholeiitic intrusions (cf. Brown, 1957; Hess, 1960).

iv) Ferrohypersthene-Eulite in Rhyolitic Pitchstones

Orthopyroxene phenocrysts in the rhyolitic pitchstones are Fe-rich (Fig. 5.12) and many in fact lie outside the experimentally determined stability field of pyroxenes in the iron-rich portion of the pyroxene quadrilateral at 1 bar and 925°C (Smith, 1972). Estimated liquidus temperatures of the rhyolitic rocks (900°-1000°C; Section 5.4) suggest that this is a reasonable estimate of the temperature of appearance of these orthopyroxenes and in any case the effects of temperatures on the stability field of iron-rich orthopyroxenes are quite small (decreasing approximately 4 mol % Fe per 100°C rise in temperature). The appearance of orthopyroxene rather than the assemblage Fe-rich olivine + quartz (or at least Fe-rich olivine + siliceous liquid) is therefore of special interest, especially in view of the low oxygen fugacities proposed for the host rocks. Carmichael (1967b) has found that, applying the oxygen geobarometer of Buddington and Lindsley (1964), orthopyroxene-bearing acid eruptives crystallized at consistently higher f_{O_2} (close to the Ni-NiO buffer curve) than compositionally equivalent rocks bearing fayalitic olivine which plot close to the faylite-magnetite-quartz buffer curve.

Two major controls on the appearance of orthopyroxene have

probably been silica activity and total pressure during crystallization. The abundance of quartz phenocrysts in most rhyolites indicates that silica activity was at a maximum. On the other hand, the experimental data of Smith (1971,1972) was obtained on stoichiometric pyroxene compositions where a_{SiO_2} would be considerably lower. From the equation:

$$2FeSiO_3 = Fe_2SiO_4 + SiO_2,$$

increased a_{SiO_2} would favour the stabilization of orthopyroxene relative to fayalitic olivine (Lindsley and Munoz, 1969).

Progressively more iron-rich orthopyroxene is stable with increasing total pressure until pure orthoferrosilite stabilizes at 14 kb. Therefore it is also possible that these pyroxenes crystallized at somewhat elevated pressures. Even neglecting the effects of a_{SiO_2}, a total pressure of 2-3 kb should stabilize these pyroxenes. Subsequent eruption and quenching must have been sufficiently rapid to prevent any significant breakdown of ferrohypersthene to Fa-rich olivine under surface conditions.

The absence of Fe-rich pigeonite in these rocks reflects the Ca-poor, peraluminous nature of the host rocks, most of which contain a trace of normative corundum.

5.3 IRON TITANIUM OXIDES

Ilmenite is ubiquitous throughout the high-Si series as either a phenocryst or groundmass phase in contrast to titanomagnetite which has been identified in only two rocks for which microprobe data are available. In the low-Si series there is a progressive variation in the nature of the

opaque oxide assemblage with increasing Mafic Index (M.I. = $100(FeO+Fe_2O_3)/FeO+Fe_2O_3+MgO$; see Chapter 6) of the host rock, namely ilmenite alone, to ilmenite plus magnetite, and finally to magnetite alone.

Cr-rich spinel occurs as small inclusions in olivine and plagioclase phenocrysts in the more mafic members of both series.

Extremely minute opaque oxide grains also abound in the dusty interstitial residuum so common in many tholeiitic rocks of the Shield, especially those belonging to the low-Si series.

TITANOMAGNETITE

As noted above, a spinel phase only appears part way through the low-Si series, titanomagnetite, so far as can be ascertained, being totally absent from rocks with M.I. <70 which dominate the low-Si series. Titanomagnetite first appears at about this stage as small groundmass grains and thereafter crystallizes earlier and more abundantly with progressive increase in M.I. of the host.

Microprobe analyses of titanomagnetites from both series are set down in Table 5.3. Analyses have been recalculated according to the method of Carmichael (1967b) on both the ilmenite and the ülvospinel bases to provide a check on analytical quality and to enable recasting into end members. All analysed grains are homogeneous one-phase spinels within the limits imposed by the resolution of the microprobe and reflected light examination. Unmixing and subsequent oxidation of ilmenite lamellae on the (111) planes of the host spinel, relatively common features of titanomagnetites in many basaltic rocks (Buddington and Lindsley, 1964; Carmichael, 1967a) have not been observed.

TABLE 5.3

MICROPROBE ANALYSES OF TITANOMAGNETITES

	1	2	3	4	5	6	7
SiO_2	0.17	0.26	0.33	-	0.28	1.38	0.54
TiO_2	26.08	27.36	25.05	24.10	26.42	27.73	24.38
Al_2O_3	1.48	0.65	1.99	0.99	1.66	1.27	0.49
Cr_2O_3	-	-	0.26	-	0.26	-	-
FeO	68.27	66.93	66.65	70.19	66.72	65.78	67.93
MnO	0.61	0.66	0.50	0.56	0.45	0.55	0.66
MgO	1.65	0.82	2.17	0.68	0.81	0.80	0.21
CaO	0.15	0.14	0.14	0.13	0.11	0.12	0.11
Total	98.41	96.82	97.09	96.65	96.45	97.63	94.32
Ilmenite basis							
FeO	36.72	32.50	35.48	37.01	37.81	38.82	38.28
Fe_2O_3	35.07	37.69	34.64	36.87	32.13	29.96	35.29
Total	101.93	100.08	100.56	100.34	99.93	100.63	99.96
Ulvöspinel basis							
FeO	52.49	54.29	50.76	51.45	53.87	56.56	53.78
Fe_2O_3	17.54	14.05	17.66	20.82	14.28	10.26	18.06
Total	100.17	98.23	98.86	98.73	98.14	98.67	98.23
Mol.% Ulsp.	72.6	78.6	71.8	68.3	75.7	82.8	73.3

KEY TO TABLE 5.3

1. Groundmass titanomagnetite in aphyric low-Si tholeiitic andesite 28050 (Table 6.1, Anal. 5).

2. Groundmass titanomagnetite in low-Si tholeiitic andesite 28051 (Table 6.1, Anal. 6).

3. Titanomagnetite microphenocryst in low-Si tholeiitic andesite 28055 (Table 6.1, Anal. 9).

4. Groundmass titanomagnetite in low-Si tholeiitic andesite 27291 (Table 6.1, Anal.15).

5. Groundmass titanomagnetite in high-Si tholeiitic andesite 28063 (Table 6.2, Anal. 3).

6. Titanomagnetite included in olivine in icelandite 28067 (Table 6.2, Anal. 7).

7. Groundmass titanomagnetite in rhyodacite 28074 (Table 6.2, Anal. 14).

No significant compositional variation is evident within or between phenocryst and groundmass crystals and tabled analyses represent averages of three to five points in one or more grains. The analyses are comparable to spinels of many mafic volcanics of alkaline and tholeiitic affinities (Carmichael, 1967a; Smith and Carmichael, 1969; Lowder, 1973; Wass 1973) although the exceptionally high ülvospinel contents of the Tweed titanomagnetites (68-84 mol %; Fig. 5.15) are worthy of note.

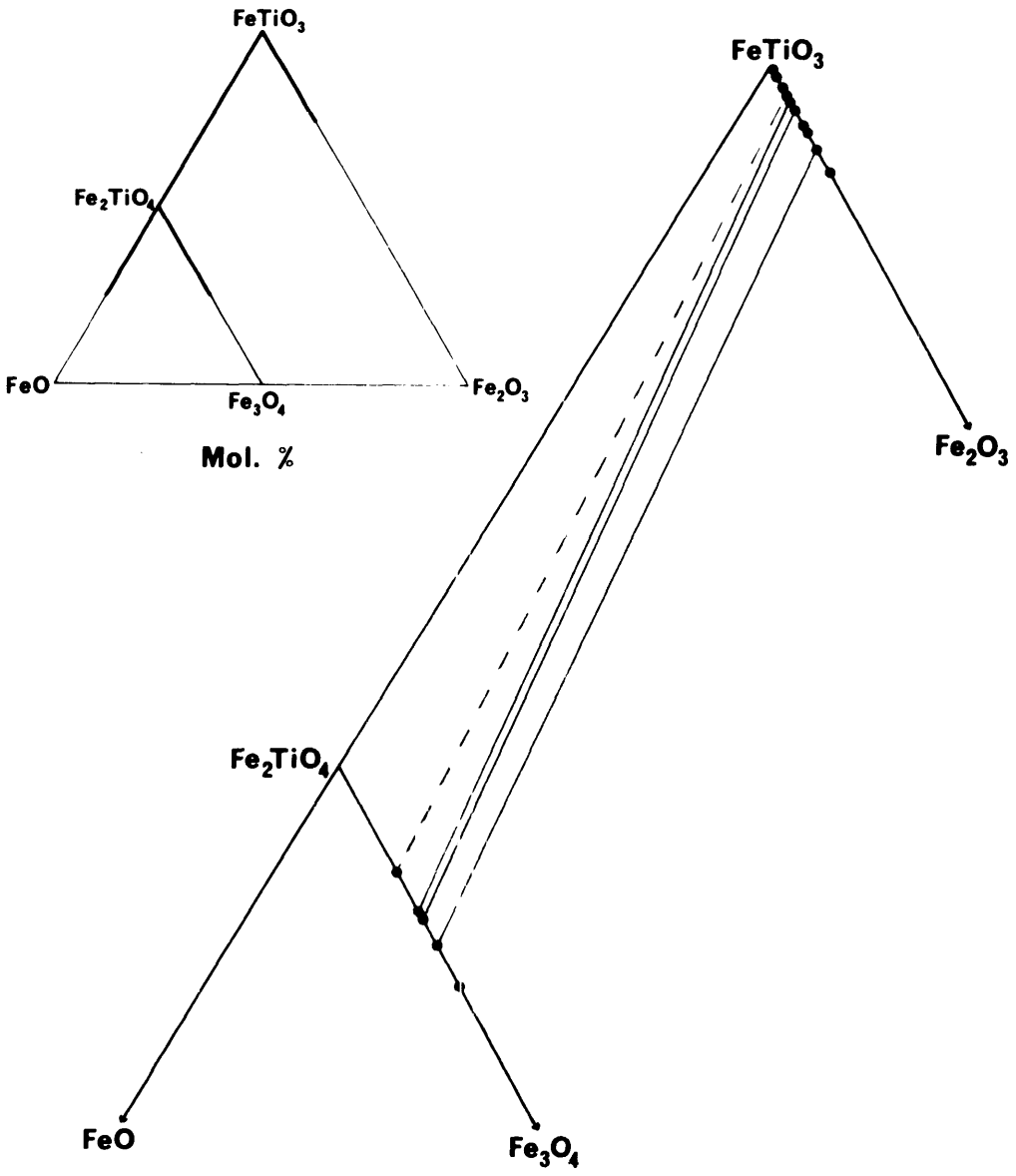

Fig. 5.15: Plot of analysed titanomagnetites (recalculated to magnetite and ulvöspinel end-members) and ilmenite (recalculated to ilmenite and hematite end-members). Unbroken tie-lines join coexisting Fe-Ti oxide pairs. Broken line joins titanomagnetite and ilmenite in icelandite 28067 (see text).

ILMENITE

In the low-Si series, ilmenite commonly occurs as somewhat ragged groundmass plates which formed late in the crystallization sequence. In contrast it forms scattered phenocrysts in most high-Si series rocks. The phenocrysts are euhedral, somewhat elongate and up to 1 mm in length. They tend toward a skeletal habit, frequently including patches of glass. Groundmass ilmenite in these rocks is somewhat more equant. All ilmenites exhibit strong anisotropy and pleochroism in reflected light.

Ilmenite analyses are presented in Table 5.4 together with recalculated values for FeO and Fe_2O_3 (Carmichael, 1967b), assuming perfect stoichiometry between Fe_2O_3 and $FeTiO_3$.

Recalculated analyses indicate a low R_2O_3 component (Fig. 5.15) and accord with high ülvospinel content of the spinel phase (where these coexist). These and other petrogenetic indicators collectively indicate relatively dry magmas with low oxygen fugacities.

COEXISTING Fe-Ti OXIDES

The presence of coexisting ilmenite and magnetite permits estimates of temperature and f_{O_2} operative during the crystallization of these phases using the data of Buddington and Lindsley (1964). This oxygen geobarometer has been widely employed in studies of volcanic rocks (Carmichael, 1967a,b; Anderson, 1968; Smith and Carmichael, 1969; Lowder, 1970,1973; Wilkinson, 1971; Anderson and Wright, 1972; Wass, 1973). Many of these studies show a close relationship between the f_{O_2}-T conditions so derived and the fayalite-magnetite-quartz (F-M-Q) oxygen buffer (Eugster and Wones, 1962; Wones and Gilbert, 1969) and indicate control of f_{O_2} by this buffer

TABLE 5.4

MICROPROBE ANALYSES OF ILMENITES

	1	2	3	4	5	6	7	8	9
TiO_2	50.92	49.94	50.19	51.85	49.32	52.17	52.61	51.81	49.85
FeO*	47.08	46.61	47.00	45.78	48.06	45.35	43.15	44.93	47.60
MnO	0.53	0.41	0.58	0.58	0.54	0.54	0.54	0.44	0.46
MgO	1.28	1.56	1.57	1.45	1.53	1.83	3.04	2.13	0.40
CaO	0.22	0.23	0.28	0.15	0.16	0.13	0.15	0.13	0.22
Total	100.03	98.75	99.62	99.81	99.61	100.02	99.49	99.44	98.53
Ilmenite basis									
FeO	42.69	41.41	41.39	43.25	40.86	42.94	41.16	42.18	43.47
Fe_2O_3	4.88	5.77	6.23	2.81	7.99	2.68	2.22	3.05	4.70
Total	100.52	99.32	100.24	100.09	100.40	100.29	99.72	99.74	99.10
Mol % R_2O_3	4.58	5.47	5.85	2.64	7.49	2.51	2.07	2.86	4.51
T (°C)			1040	950				940	
log f_{O_2}			-10.9	-12.8				-13.0	

	10	11	12	13	14	15	16	17	18
TiO_2	51.74	52.11	49.19	51.32	51.18	51.88	53.15	51.61	50.94
FeO*	45.81	45.54	46.56	46.75	46.89	45.90	45.94	46.54	46.33
MnO	0.45	0.48	0.43	0.70	0.64	0.69	0.64	0.54	0.53
MgO	1.21	0.62	2.35	0.32	1.38	1.12	0.70	0.34	0.61
CaO	0.12	0.22	0.14	-	-	0.08	0.13	0.09	-
Total	99.33	98.97	98.67	100.09	100.09	99.67	100.56	99.12	98.41
Ilmenite basis									
FeO	43.77	44.99	39.42	44.43	42.92	43.86	45.73	45.14	44.18
Fe_2O_3	2.27	0.61	7.93	2.58	4.41	2.27	0.23	1.55	2.39
Total	99.56	99.03	99.46	100.35	100.53	99.90	100.58	99.27	98.65
mol % R_2O_3	2.15	0.58	7.47	2.44	4.13	2.14	0.21	1.48	2.30
T (°C)	(1025)								
log f_{O_2}	(-11.7)								

KEY TO TABLE 5.4

1. Groundmass ilmenite in low-Si tholeiitic andesite 28048 (Table 6.1, Anal. 3).

2. Groundmass ilmenite in low-Si tholeiitic andesite 28049 (Table 6.1, Anal. 4).

3. Groundmass ilmenite in low-Si tholeiitic andesite 28050 (Table 6.1, Anal. 5).

4. Groundmass ilmenite in low-Si tholeiitic andesite 28051 (Table 6.1, Anal. 6).

5. Groundmass ilmenite in high-Al tholeiitic andesite 27290 (Table 6.1, Anal. 14).

6. Ilmenite phenocryst in high-Si tholeiitic andesite 28061 (Table 6.2, Anal. 1).

7. Ilmenite phenocryst in high-Si tholeiitic andesite 28062 (Table 6.2, Anal. 2).

8. Groundmass ilmenite in high-Si tholeiitic andesite 28063 (Table 6.2, Anal. 3).

9. Ilmenite microphenocryst in high-Si tholeiitic andesite 28065 (Table 6.2, Anal. 5).

10. Ilmenite phenocryst in icelandite 28067 (Table 6.2, Anal. 7).

11. Groundmass ilmenite in icelandite 28070 (Table 6.2, Anal. 10).

12. Ilmenite microphenocryst in icelandite 28071 (Table 6.2, Anal. 11).

13. Ilmenite microphenocryst in icelandite 28072 (Table 6.2, Anal. 12).

14. Ilmenite microphenocryst in rhyodacite 28073 (Table 6.2, Anal. 13).

15. Ilmenite microphenocryst in rhyolitic pitchstone 28075 (Table 6.3, Anal. 1).

16. Ilmenite microphenocryst in rhyolitic pitchstone 28076 (Table 6.3, Anal. 2).

17. Ilmenite microphenocryst in rhyolitic pitchstone 28078 (Table 6.3, Anal. 4).

18. Ilmenite microphenocryst in rhyolitic pitchstone 28079 (Table 6.3, Anal. 5).

* Total Fe as FeO.

assemblage.

Unfortunately, analyses of undoubted coexisting ilmenite-magnetite pairs have only been obtained on three Tweed volcanics, two from the low-Si and one from the high-Si series. Another from the high-Si series (28067) has ilmenite phenocrysts and magnetite included in olivine but it is by no means certain that these comprise a coexisting equilibrium pair. On an f_{O_2}-T diagram (Eugster and Wones, 1962) these rocks occupy a position approximately parallel to but displaced significantly downward from the F-M-Q buffer curve and in fact indicate conditions intermediate between this and the magnetite-wüstite buffer (Fig. 5.16). This suggests somewhat lower f_{O_2} conditions than those indicated for other tholeiitic rocks (Peck *et al.*, 1964; Carmichael, 1967a; Evans and Moore, 1968; Smith and Carmichael, 1969; Anderson and Wright, 1973) and also those obtained by direct measurement in a Kilauea lava lake (Peck and Wright, 1966) and by experiment (Fudali, 1965) which all fall on or near the F-M-Q curve.

FACTORS CONTROLLING PRECIPITATION OF THE Fe-Ti OXIDES

The pattern of occurrence of ilmenite and magnetite in both series warrants further comment. The striking predominance of ilmenite over titanomagnetite in all high-Si series rocks and in all but the most iron-rich low-Si series rocks is somewhat unique relationship since in most other tholeiitic series the rhombohedral phase generally coexists with a spinel e.g. Thingmuli (Carmichael, 1967a).

Considering firstly the absence of ilmenite from the most iron-rich members of the low-Si series, a possible explanation lies in the very

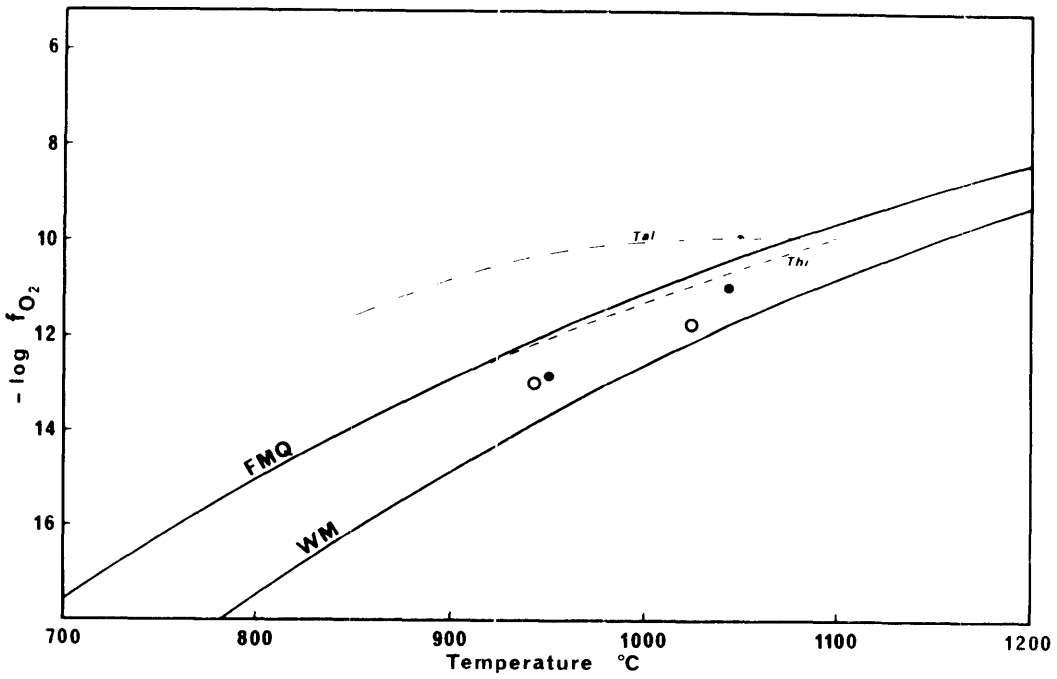

Fig. 5.16: Plot of log f_{O_2} against temperature deduced from coexisting Fe-Ti oxide pairs from rocks of the low-Si (filled circles) and high-Si (open circles) series. The curves FMQ and WM represent the buffer assemblages fayalite-magnetite-quartz and wüstite-magnetite respectively. Generalized curves for the Thingmuli (Thi; Carmichael, 1967a) and Talasea (Tal; Lowder, 1970) volcanic series are shown for comparison.

small primary phase areas of rhombohedral phases in the system MgO-Fe oxide-TiO_2 at 1 bar in air (Woermann *et al.*, 1969), in contrast to spinel which has a large primary phase volume. In the system $MgO-FeO-Fe_2O_3-CaAl_2Si_2O_8-SiO_2$ (Roeder and Osborn, 1966) the stability field of magnetite expands with increasing f_{O_2}. A similar trend is observed in natural rock compositions (Nesbitt and Hamilton, 1969; Holloway and Burnham, 1972; Helz, 1973). The absence of ilmenite therefore probably reflects conditions of somewhat elevated f_{O_2} relative to the less iron-rich members of the series. The regular variation in the Fe-Ti oxide assemblage in the low-Si series may represent a regular increase in f_{O_2} with increasing Mafic Index, due to continued fractionation of Fe^{2+} in olivines and pyroxenes under more or less closed system conditions (Carmichael and Nicholls, 1967).

Following from the above, the predominance of ilmenite in the high-Si series may have resulted from relatively low Fe^{3+} concentrations in the melts, brought about by low f_{O_2} relative to the F-M-Q buffer. On the other hand TiO_2, while being lower than in most members of the low-Si series, has probably been sufficient in these more acidic rocks to induce precipitation of R_2O_3-poor ilmenite (Carmichael and Nicholls, 1967). If so, there must be a significant increase in the primary rhombohedral phase volume under these conditions over that determined in the system MgO-Fe oxide-TiO_2 in air (Woermann *et al.*, 1969), evidently reflecting a combination of reduced f_{O_2} and the more complex nature of the poly-component natural rock system. It is worthy of note that ilmenite is the dominant Fe-Ti oxide in two Snake River basaltic rocks crystallizing at various pressures (Thompson, 1972b) under conditions appropriate to the wüstite-magnetite buffer (Thompson and Kushiro,

1972) with magnetite appearing in only one rock and then as a near-solidus phase.

MINOR ELEMENTS IN THE Fe-Ti OXIDES

Entry of minor elements into spinel and rhombohedral phases in general accords with previous data. Mg, Mn, and Ca are consistent minor components of both phases; significant amounts of Al and minor Cr and Si occur in the spinel phase but in the rhombohedral phase these elements are below the limits of detection.

The Mg contents of both ilmenite and magnetite are to some extent dependent upon host rock compositions and order of crystallization. Thus in the high-Si series where ilmenite generally forms phenocrysts MgO (in a geikielite component) is higher in rocks with the lowest Mafic Indices and is indeed somewhat higher in these rocks than in the most magnesian low-Si series rocks where it crystallizes subsequent to ferromagnesian silicates.

CHROMIAN SPINEL INCLUSIONS IN PLAGIOCLASE AND OLIVINE

Small chromian spinel euhedra are commonly included in plagioclase and olivine phenocrysts in the more basic rocks of both series. Analyses of two of these inclusions are presented in Table 5.5. They are essentially identical in occurrence and composition to many described elsewhere (Evans and Moore, 1968; Evans and Wright, 1972; Wass, 1973) and little further discussion is warranted. In essence they are a solid solution between spinel ($MgAl_2O_4$) and Fe-chromite ($FeCr_2O_4$) with a minor Mg-chromite ($MgCr_2O_4$) component. Their origin has been reviewed in some detail by Wass (1973) who concludes that in alkaline rocks of the Southern Highlands of N.S.W. Cr-spinel

TABLE 5.5

MICROPROBE ANALYSES OF CHROMIAN SPINELS

	1	2
SiO_2	-	0.20
TiO_2	2.74	2.53
Al_2O_3	19.48	20.06
Cr_2O_3	37.31	36.81
FeO*	32.32	28.96
MnO	0.09	0.21
MgO	7.85	10.54
CaO	0.16	0.28
Total	99.95	99.59
Ulvöspinel basis		
FeO	25.43	21.13
Fe_2O_3	7.65	8.71
Total	100.71	100.47
Mol. % End Members		
Fe_2SiO_4	-	0.7
Fe_2TiO_4	7.3	6.7
$CaAl_2O_4$	0.6	1.1
$MnAl_2O_4$	0.3	0.6
$MgAl_2O_4$	39.7	39.8
$MgCr_2O_4$	1.7	15.3
$FeAl_2O_4$	-	-
$FeCr_2O_4$	50.5	35.8

1. Chromian spinel included in olivine in low-Si tholeiitic andesite 28048 (Table 6.1, Anal. 3).

2. Chromian spinel included in plagioclase in low-Si tholeiitic andesite 28048.

* Total Fe as FeO.

is an early liquidus phase along with olivine. A similar conclusion is acceptable here although the presence of Cr-spinel in many plagioclase phenocrysts with or without olivine is an associated phenocryst phase obviously suggests that the accompanying crystallization of olivine is not essential.

The conditions of low f_{O_2} implied for most Tweed rocks ($\sim 10^{-11}$ at 1050°C) accords well with the suggestion that precipitation of Cr-spinel is favoured by low f_{O_2} and relatively high temperatures (Roeder and Emslie, 1970).

5.4 FELDSPARS

Plagioclase is an abundant groundmass constituent throughout both the low-Si and the high-Si series and also occurs as phenocrysts in many of the rocks. Alkali feldspar is virtually absent from the low-Si series and intermediate members of the high-Si series but is a common phenocryst species in rhyolitic rocks.

Microprobes analyses of phenocryst and groundmass feldspars from twenty-five rocks representative of the two series provide information on compositional variation within individual phenocrysts and within individual specimens throughout the two series. Feldspars were analysed for SiO_2, Al_2O_3, total Fe (recorded as Fe_2O_3), CaO, Na_2O and K_2O. Minor elements (namely Mg, Ti, Mn) are below the sensitivity limit of the microprobe. The feldspar analyses are set down in Table II.3 (Appendix II). A summary of microprobe data on analysed rocks (supplemented by optical data) is presented in Table 5.6 and illustrated in Figure 5.17.

5.4.1 Feldspars in the Low-Si Series

Plagioclase: Most members of the low-Si series contain at least

TABLE 5.6

SUMMARY OF MICROPROBE DATA ON PLAGIOCLASES IN THOLEIITIC ROCKS OF THE TWEED SHIELD

Specimen No.	Compositional Range (100 An/Ab+An) Phenocrysts	Groundmass
28048	67 - 63	60 - 50
28049	53 - 44	56 - 42
28050		54 - 43
28051	55 - 45	43 - 34
28055	60 - 40	43 - 38
27291	48 - 43	43 - 40
28061	65 - 58 23 - 20*	57 - 31
28062	56 - 48	59 - 45
28063	40 - 39	45 - 43
28065	65 - 58	57 - 31
28067	39 - 33 47 - 30*	43 - 30
28070	61 - 43	57 - 45
28071	62 - 58 29 - 27*	57 - 36
28072	33 - 29 48 - 27* 24 - 22*	50 - 32
28073	40 - 35	39 - 31
28074	37 - 35	47, 23
28075	31 - 23	52 - 47
28076	31 - 24	24
28078	30 - 25	
28079	27 - 24	
28084	27 - 26	28
28088	25 - 22	

* Reverse zoned, or sieved type - see text.

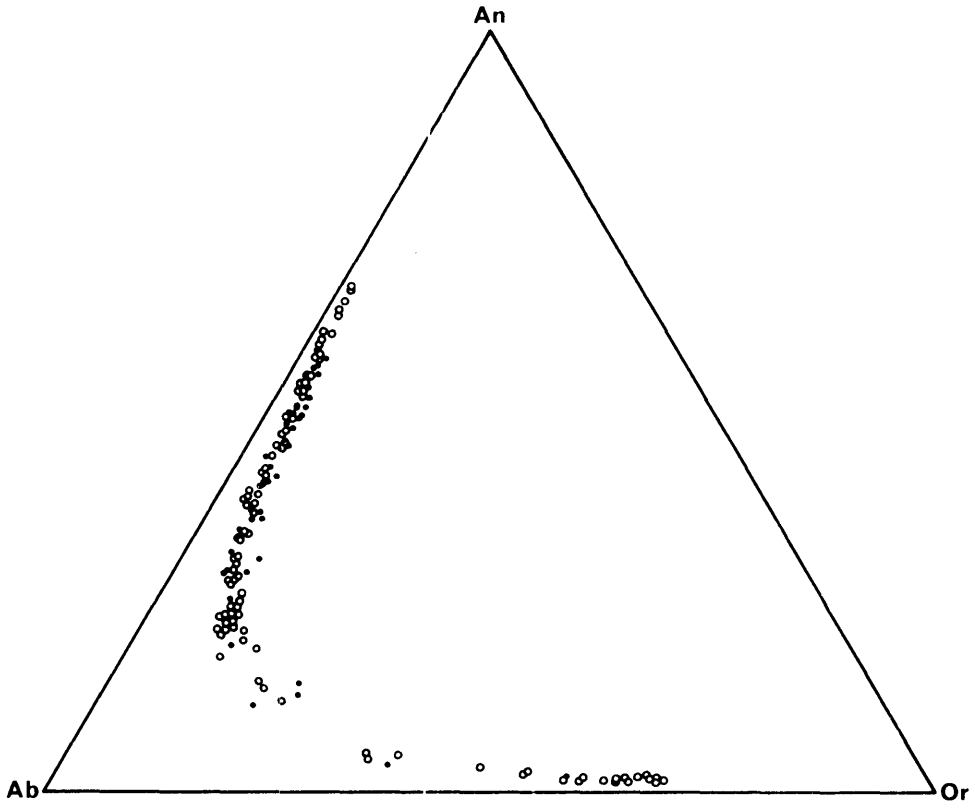

Fig. 5.17: Collation of all microprobe data on feldspars from tholeiitic volcanics of the southern portion of the Tweed Shield plotted in terms of Ab, An and Or (wt %). Open circles, feldspar phenocrysts; filled circles, groundmass feldspars.

occasional plagioclase phenocrysts and a significant proportion of these rocks (about 10%) are strongly porphyritic in plagioclase. Phenocrysts vary widely in size, shape and composition. High-alumina variants of the low-Si series (27290) contain abundant, very large (up to 2 cm) and virtually unzoned plagioclase megacrysts interpreted as moderately high pressure cognate phases (Duggan and Wilkinson, 1973). In most low-Si rocks plagioclase phenocrysts are about 1-3 mm in length and constitute about 1-5% of the mode. They are usually euhedral to subhedral and characteristically quite fresh and glassy even though the host is commonly altered. Zoning in most phenocrysts is normal and of restricted range, involving no more than 3-5 wt % An.

Distinctive phenocrysts occur in some members of the low-Si series. These have glassy, unzoned, relatively sodic cores ($\sim An_{30}$-An_{40}), surrounded by spongey reaction zones of more calcic plagioclase ($\sim An_{50}$). These phenocrysts are commonly subhedral to anhedral and extensively resorbed. The textural features of these phenocrysts are essentially identical with those of andesine, oligoclase and anorthoclase megacrysts in alkaline rocks from numerous localities (Wright, 1968; Binns *et al.*, 1970; Laughlin *et al.*, 1974) and in some tholeiitic andesites from southern Utah (Lowder, 1973) although the Tweed feldspars are much smaller than these, rarely exceeding 3 mm in diameter. The genesis of these phenocrysts will be considered in a subsequent chapter.

Figure 5.18 is a plot of microprobe analyses of feldspars in the low-Si series. Throughout the series phenocrysts vary from calcic labradorite to intermediate andesine and groundmass crystals vary from intermediate labradorite to sodic andesine. Feldspar microprobe data for individual rocks

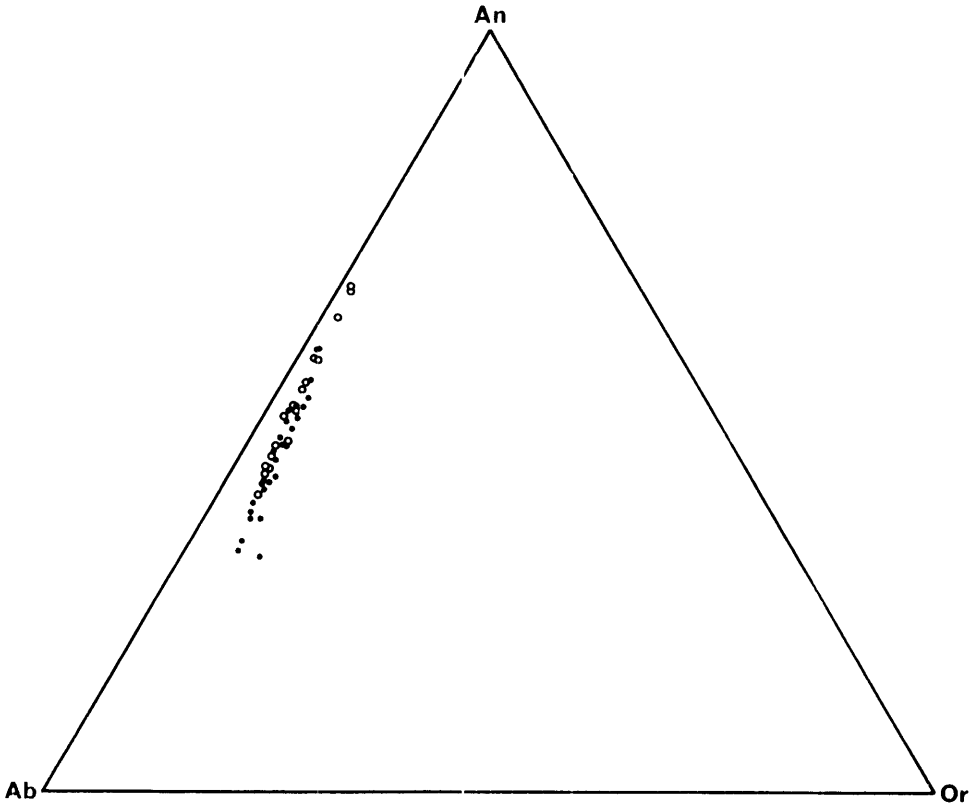

Fig. 5.18: Collation of microprobe data on feldspars from rocks of the low-Si series plotted in terms of Ab, An and Or (wt %). Open circles, feldspar phenocrysts; filled circles, groundmass feldspars.

are plotted in Figure 5.19, together with the C.I.P.W. normative feldspar composition of the host. Within an individual specimen, phenocryst and groundmass compositions sometimes overlap considerably and groundmass grains may be more calcic then phenocrysts (e.g. 28049; Table 5.6). However this is more prevalent in plagioclase of the high-Si series described below.

Alkali Feldspar: In some low-Si lavas, particularly those containing only minor residual glass, small irregular colourless areas of low relief and low birefringence in the groundmass suggest the presence of alkali feldspar. Microprobe surveys of the groundmass of these rocks indicate that although alkali feldspar is present it is in fact quite rare. An analysis of one such alkali feldspar is presented in Table II.3 (Appendix II).

5.4.2 Feldspars of the High-Si Series (Excluding Rhyolites)

Plagioclase: Plagioclase in the intermediate members of the high-Si series tholeiitic andesite → tholeiitic rhyodacite vary in composition from labradorite through andesine and potash oligoclase to lime anorthoclase. These feldspars are essentially similar in composition and textural characteristics to those already described in the low-Si series. However a larger proportion of the high-Si lavas (>90%) are to some extent porphyritic in plagioclase which has probably been a liquidus or near liquidus phase in all lavas belonging to this series.

Analysed feldspars from rocks of the high-Si series are plotted on Figure 5.20 and data for individual rocks plotted on Figure 5.21. In common with the low-Si series feldspars, normally zoned phenocrysts show only very restricted zoning. Many rocks contain reverse zoned and sieved phenocrysts. In addition, phenocrysts and groundmass grains overlap considerably in

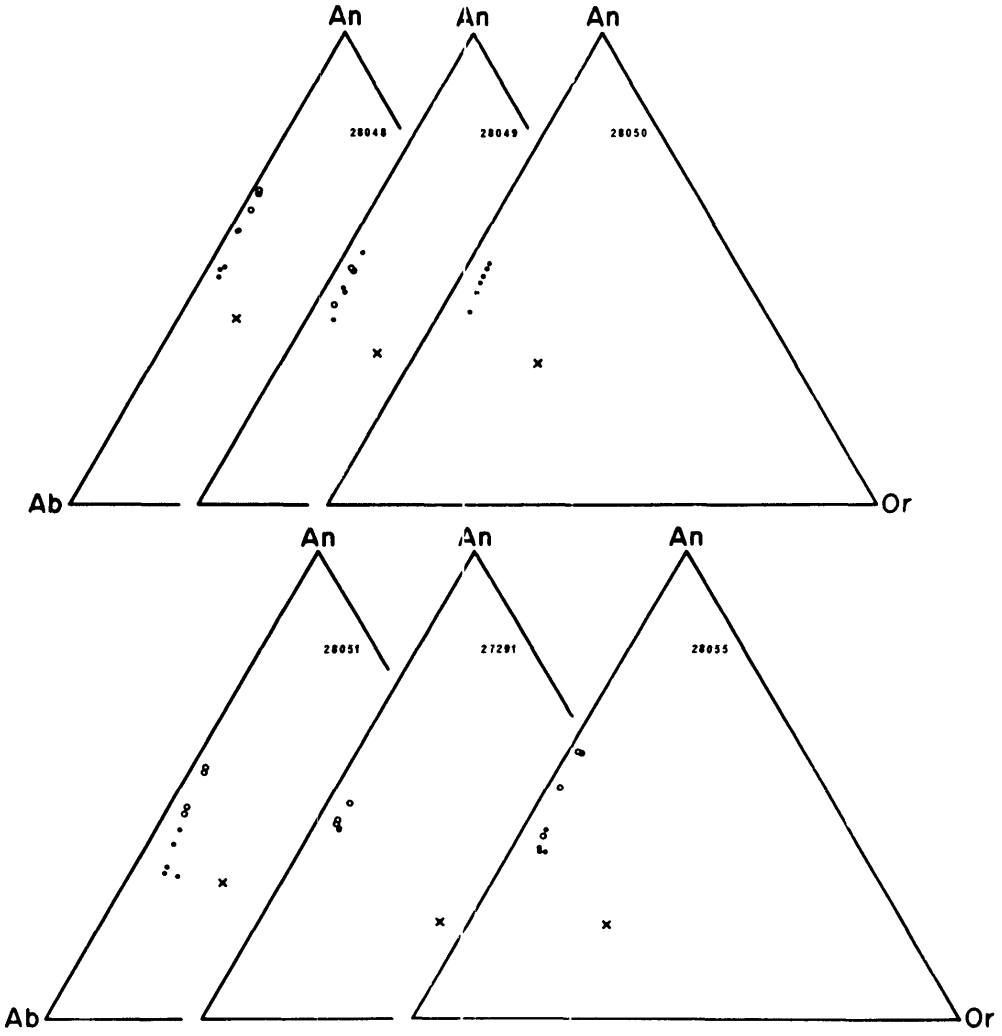

Fig. 5.19: Analysed feldspars from individual rocks of the low-Si series plotted in terms of Ab, An and Or (wt %). Open circles, feldspar phenocrysts; filled circles, groundmass feldspars; crosses, normative feldspar composition of host rock.

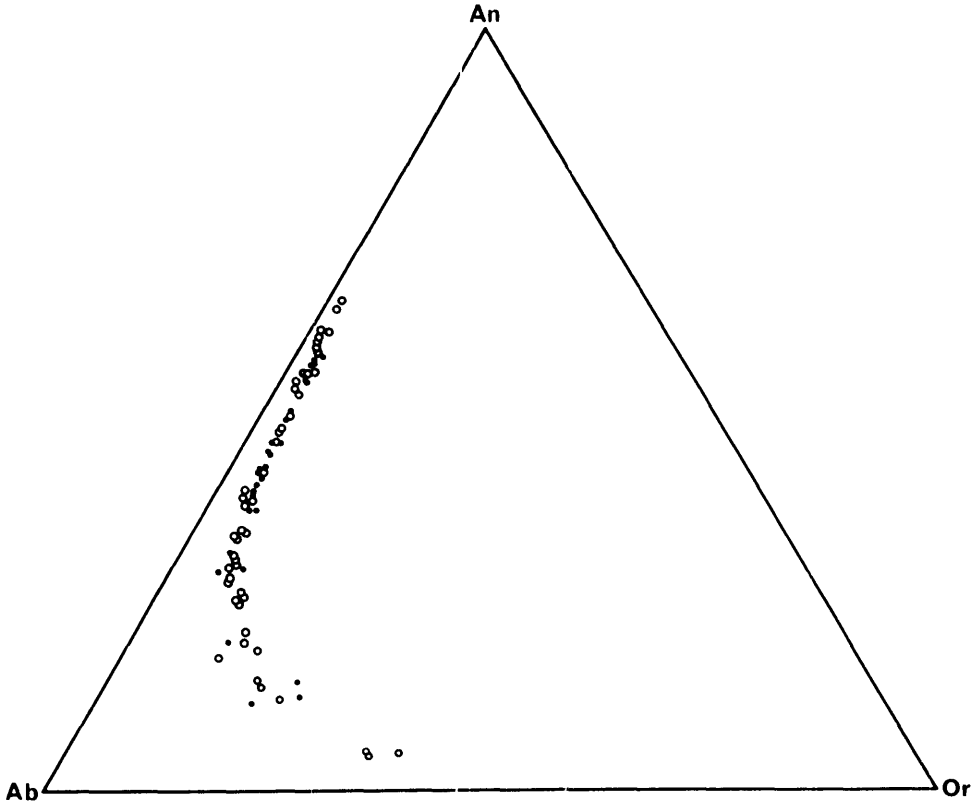

Fig. 5.20: Collation of microprobe data on feldspars from rocks of the high-Si series plotted in terms of Ab, An and Or (wt %). Open circles, feldspar phenocrysts; filled circles, groundmass feldspars.

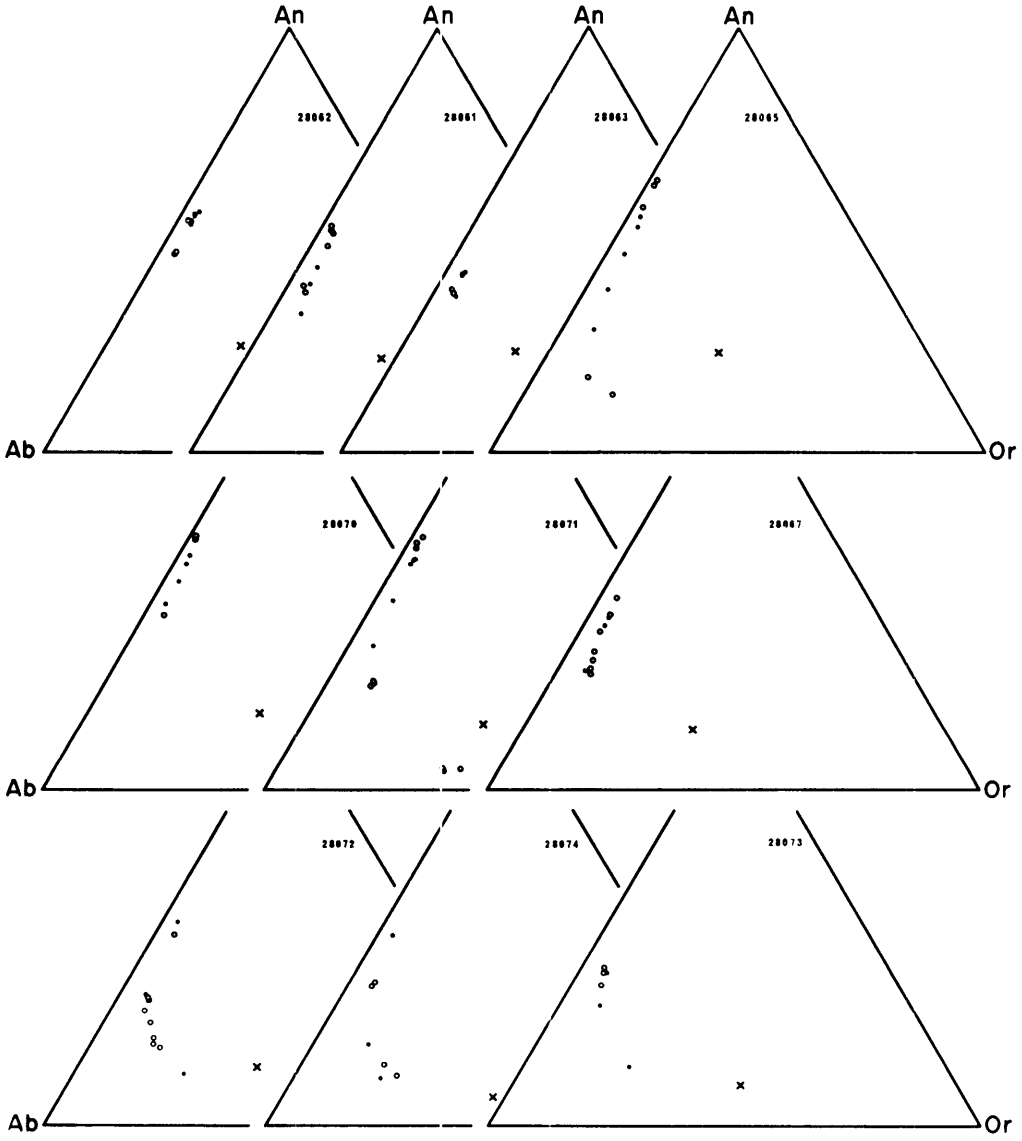

Fig. 5.21: Analysed feldspars from individual rocks of the high-Si series plotted in terms of Ab, An and Or (wt %). Open circles, feldspar phenocrysts; filled circles, groundmass feldspars; crosses, normative feldspar composition of host rock.

composition in most rocks.

Sieved phenocrysts (Plate 3, No.3) are quite small (average 1 mm diameter) and invariably somewhat resorbed; however sieving tends to be on a finer scale than in feldspars in the Low-Si series. Microprobe data on some sieved phenocrysts in various tholeiitic andesite and icelandite host rocks are plotted on Figure 5.22. Unfortunately the extremely fine structure of the sieved zone generally precludes accurate microprobe analysis but one such analysis and a number of optical determinations (β = 1.550-1.555; An_{35}-An_{45}) suggest that the sieved areas have compositions not markedly dissimilar to those of the thin glassy mantles and groundmass feldspars.

The sieved nature of these phenocrysts is not ubiquitous. For example the analysed phenocryst from the tholeiitic andesite 28061 has a glassy unzoned core (An_{40}) mantled by a narrow rim of more calcic plagioclase (An_{53}). Some sieved feldspars in rocks of the high-Si series occur intergrown with or contain inclusions of ferroaugite (Plate 3, No.4).

Alkali Feldspars: Alkali feldspar phenocrysts ($Ab_{60}An_5Or_{35}$) occur in one icelandite (28071; Fig. 5.21) which however shows mineralogical and textural evidence of magma mixing or hybrid processes and hence the feldspars may not have been in equilibrium with their host liquid.

Phenocrysts plotting in the anorthoclase field are all of the sieved variety (Fig. 5.22) and possess a narrow calcic oligoclase mantle. These are probably closely related to sieved phenocrysts described previously.

5.4.3 Feldspars from the Rhyolites

Apart from a few near-aphyric representatives, all rhyolitic rocks are characterized by phenocrysts of two feldspars, namely oligoclase and

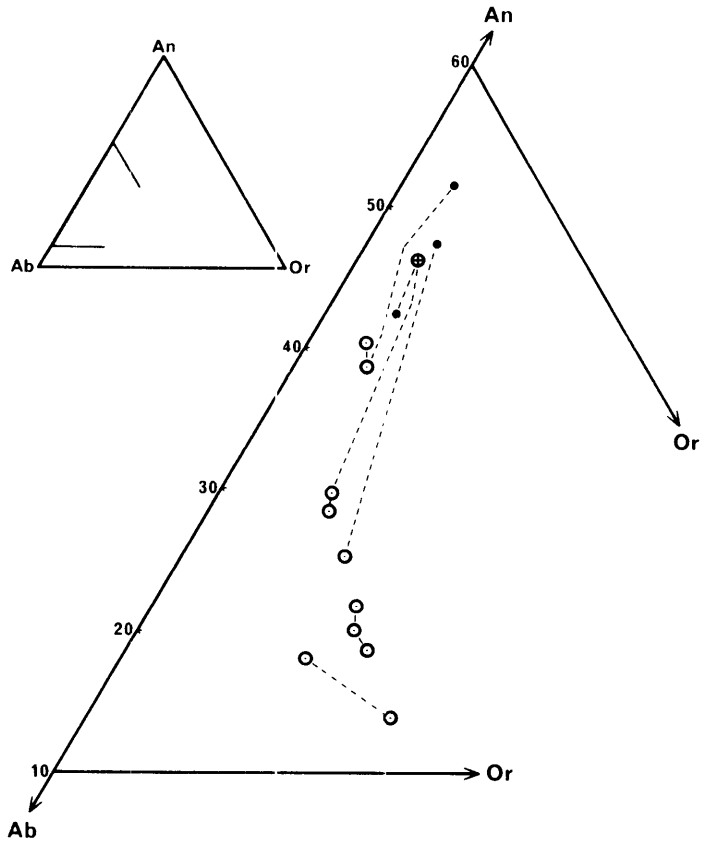

Fig. 5.22: Microprobe data on some sieved feldspars plotted in terms of Ab,An and Or (wt %). Open circles, glassy unzoned cores; ⊕, sieved portion; filled circles, glassy clear mantles of sieved phenocrysts.

sanidine, regardless of whether the host rock is glassy, devitrified or tuffaceous.

Plagioclase: Plagioclase phenocrysts in the rhyolitic rocks are small (<1 mm) and modally insignificant (generally less than 2%; Table 4.3). They show little variation in composition, invariably falling within the range $Ab_{66}An_{26}Or_8$-$Ab_{70}An_{19}Or_{10}$ wt %. Microprobe data are set down in Table II.3 (Appendix II) and summarized in Figure 5.23. Microprobe analyses of feldspars of individual rocks are plotted in Figure 5.24.

Zoning is very limited but consistently normal. Thus must phenocrysts have a core whose composition is close to $Ab_{67}An_{24}Or_9$ mantled by plagioclase, about $Ab_{68}An_{22}Or_{10}$. Entry of Fe into rhyolitic plagioclase is extremely limited and only in rare instances is the analysis for total iron (recorded as Fe_2O_3) above the sensitivity limit of the microprobe. The low Fe contents, compared with compositionally similar plagioclase in the less acid rocks, is probably a function of the relatively Fe-poor host rhyolitic liquids.

Sanidine: Sanidine phenocrysts are abundant in all rhyolitic rocks showing any significant degree of phenocryst development (Table 4.3). The abundant separation of sanidine during intratelluric crystallization is not surprising in view of the normative feldspar compositions of the rhyolitic rocks in the system Ab-An-Or (Fig. 5.23) which fall close to the Ab-Or join.

Where sanidine phenocrysts have been analysed their compositions are relatively constant. Thus the composition of the cores of phenocrysts (with the exception of one intrusive rhyolite) cluster close to the $Ab_{31}An_2Or_{67}$. Zoning is significant only in the outer 10% of the crystal and is

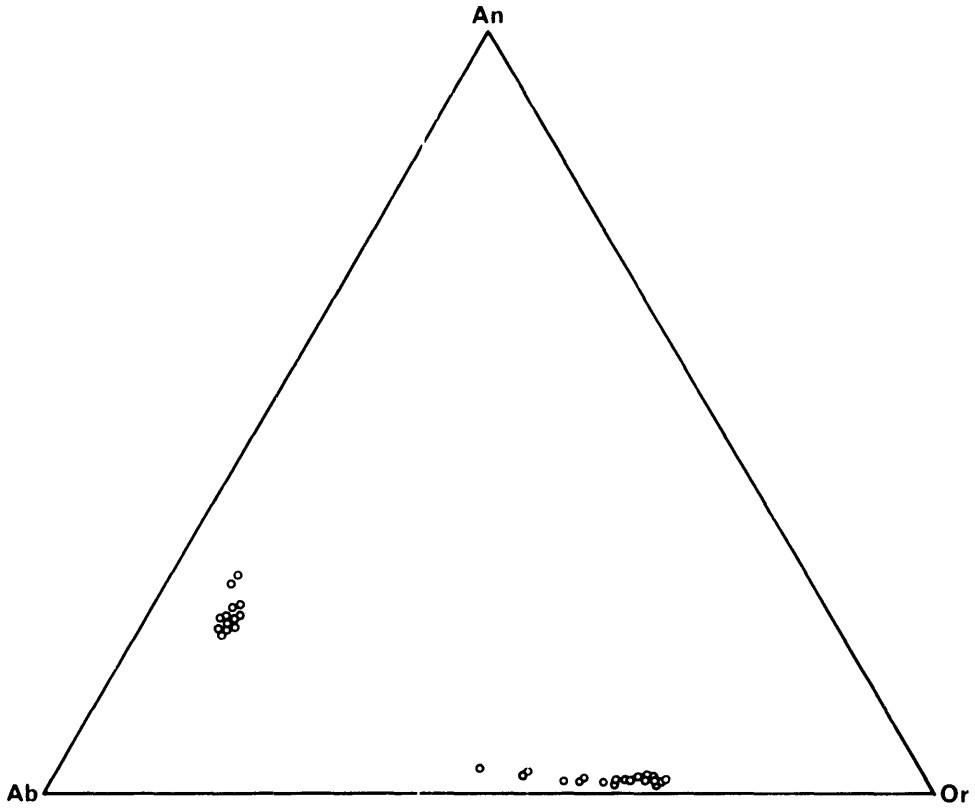

Fig. 5.23: Collation of microprobe data on feldspar phenocrysts from the rhyolitic rocks plotted in terms of Ab, An and Or (wt %).

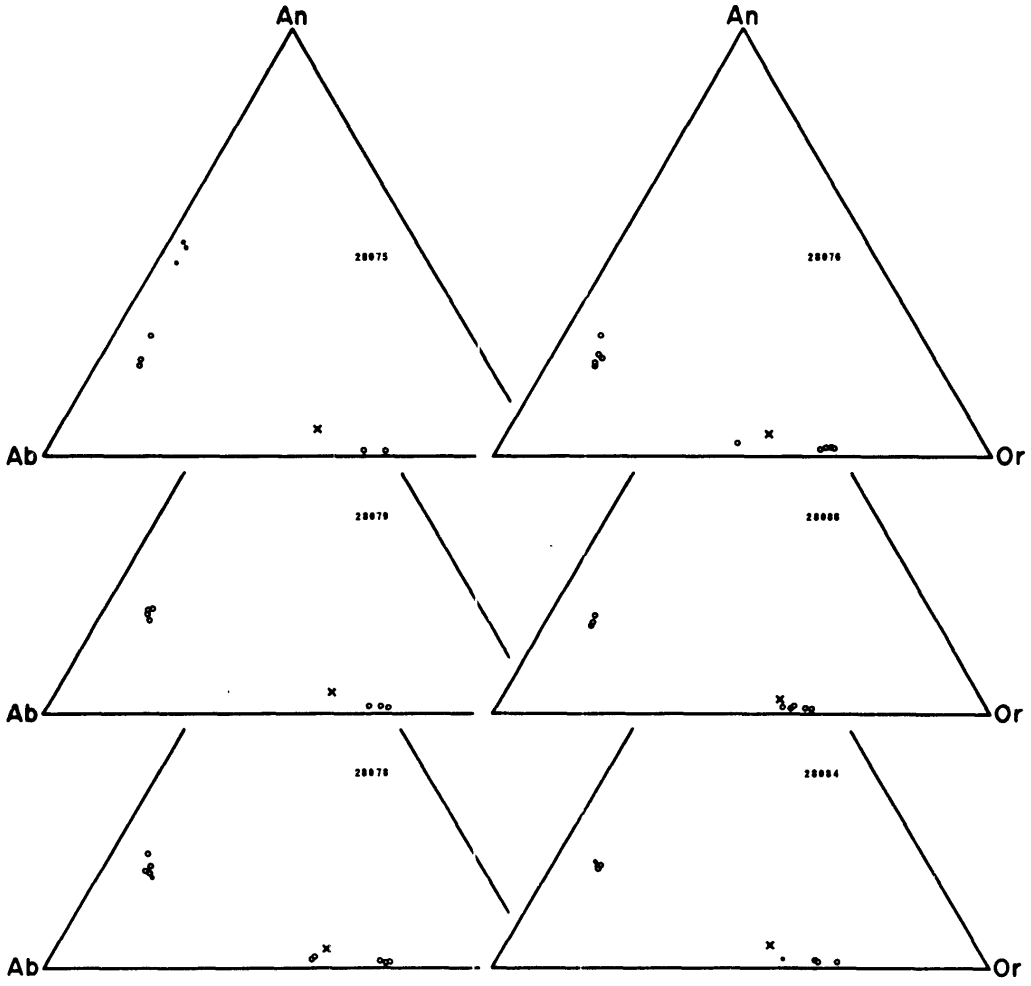

Fig. 5.24: Analysed feldspars from various rhyolites and rhyolitic pitchstones plotted in terms of Ab, An and Or (wt %). Open circles, feldspar phenocrysts; filled circles, groundmass feldspars; crosses, normative feldspar composition of host rock.

usually restricted to a decrease of about 5 wt % Or. More rarely, zoning involves a decrease in up to 20 wt % Or to about $Ab_{49}An_3Or_{48}$. More extreme zoning is restricted to the sanidines from quenched vitrophyric hosts. Subsolidus exsolution of the sanidines to form cryptoperthites is indicated by a well defined split in the $\bar{2}01$ peak in x-ray diffraction traces. However the K-rich and Na-rich phases are not resolvable by optical or microprobe techniques.

The potassic inner zones of sanidine phenocrysts were undoubtedly out of equilibrium with the residual liquids under extrusive conditions. In many phenocrysts internal resorption is common and extensive, producing a "brain structure" of glassy corrosion canals of brown glass in residual sanidine. Resorption of sanidine during crystallization appears to have taken place without subsequent making over of the sanidine cores to the more sodic compositions characteristic of the marginal zones. The compositions of the interior portions of resorbed crystals are identical to those of totally unresorbed crystals.

One notable aspect of the chemistry of the sanidine phenocrysts is their Al-excessive nature relative to a stoichiometric composition. In the sanidine analyses (Table II.3c, Appendix II), between 0.5 and 1.0 wt % Al_2O_3 remains after allotment of equivalent molecular proportions of Al_2O_3 to the molecular proportions of Na_2O, K_2O and CaO. This is unlikely to be due to analytical error since a similar excess of Al is evident in the sanidine analyses given by Carmichael (1963). This feature may have important petrogenetic implications in cases of extreme fractionation (see Section 7.5.4).

5.4.4 Discussion

i) Origin of the Sieved Phenocrysts

The genesis of large andesine phenocrysts ("megacrysts") in a high-alumina tholeiitic andesite of the low-Si series from near Brunswick Heads has already been discussed (Duggan and Wilkinson, 1973). It was proposed that these are cognate phases which crystallized from the host liquid under relatively anhydrous conditions at pressures in the vicinity of 9 kb. These feldspar megacrysts coexist with crystals of aluminian bronzite and aluminian augite whose chemistries also provide compelling evidence of high pressure crystallization. Similar Al-rich pyroxenes occur sporadically throughout the Shield in flows of low-Si tholeiitic andesite of more normal (lower Al_2O_3) chemistry. The sieved and reversed zoned types of feldspar phenocrysts commonly coexist with high pressure pyroxenes and hence a relatively high pressure origin is also suggested for these phenocrysts.

A comparable high pressure origin can probably be assigned to more or less identical sieved feldspar phenocrysts in some members of the high-Si series (Fig. 5.22). However, one important difference is apparent between the sieved phenocrysts of the low-Si and the high-Si series, namely that the latter coexist with ferroaugite poor in Al^{VI}. It will be argued in a subsequent chapter that the absence of pyroxenes of demonstrably high pressure origin from these rocks indicates crystallization under somewhat lower pressure conditions, probably in the vicinity of 5 kb. Sieved plagioclase phenocrysts in subalkaline volcanics exhibiting similar compositional trends have been recorded from a number of localities, (MacDonald and

Katsura, 1965; Wise, 1969; Doe *et al.*, 1969; Lowder, 1970,1973). These phenocrysts have usually been interpreted as xenocrysts rafted from underlying basement rocks during ascent of the magma (e.g. Doe *et al.*, 1969; Lowder, 1973). On the other hand, Wise (1969) proposed that, in essence, the sieving and associated clear margins result from crystallization at depth in a relatively dry environment followed by transport to near surface conditions leading to partial resorption of early formed crystals. Kempe and Schilling (1974) attribute resorption and reverse zoning in plagioclase phenocrysts in a basalt from Discovery Tablemount, South Atlantic Ocean, to pressure variations permitting renewed pulses of magma of varying composition.

An accidental origin for sieved phenocrysts (the more popular proposal) is considered untenable for their genesis since there is some correlation between the core compositions of these phenocrysts and the respective host rock compositions i.e. sieved plagioclases in icelandites have more sodic core compositions than those from tholeiitic andesites. Furthermore, some crystals occur intergrown with ferroaugites which are believed cognate and minor zoning in the unaltered plagioclase core is typically igneous in nature with oscillatory zoning dominant. This evidence is consistent with a cognate origin.

The model of Wise (1969) is consistent with available experimental data. For example, plagioclase crystallizing from natural rock compositions at moderately high pressures under anhydrous conditions becomes progressively more Ab-rich, relative to the plagioclase crystallizing at low pressures (Cohen *et al.*, 1967; Green, 1969; Thompson, 1972b). Lindsley (1969) has shown that although the liquidus and solidus curves in the binary Ab-An

system at 1 atmosphere (Bowen, 1913) maintain a similar configuration at pressures up to about 10 kb anhydrous they are nevertheless displaced to significantly higher temperatures. Release of pressure in a water-deficient magma following some plagioclase crystallization at depth (e.g. by rise of magma to higher levels) may lower the liquidus and solidus temperatures causing cessation of plagioclase crystallization and resorption of some of the earlier relatively Ab-rich plagioclase of high pressure crystallization. Since intracrystal diffusion of elements in plagioclase is quite slow, continuous readjustment of the total composition of a crystal within the lower pressure regime is unlikely. Consequently the earlier, higher pressure crystals may be partly resorbed. A similar effect may also be produced by a relatively small increase in P_{H_2O} (Yoder, 1969a,b).

ii) Or Contents of Plagioclase

Or contents of feldspars in the Tweed low-Si and high-Si series are plotted against An in Figure 5.25 and compared with Or/An trends in plagioclases from Makaopuhi Lava Lake, Hawaii (Evans and Moore, 1968), Hawaiian tholeiitic lavas (Keil *et al.*, 1972) and alkaline lavas of the Lake Rudolf region, East Africa (Brown and Carmichael, 1971).

Entry of Or into plagioclase varies inversely with An content as has been previously demonstrated by numerous studies of feldspars from volcanic rocks (Carmichael, 1967; Evans and Moore, 1968; Smith and Carmichael, 1968; Lowder, 1970,1973; Brown and Carmichael, 1969,1971; Keil *et al.*, 1972). This accords with the normal trend with respect to intersection of the ternary feldspar solidus and solvus surfaces in the Ab-An-Or system

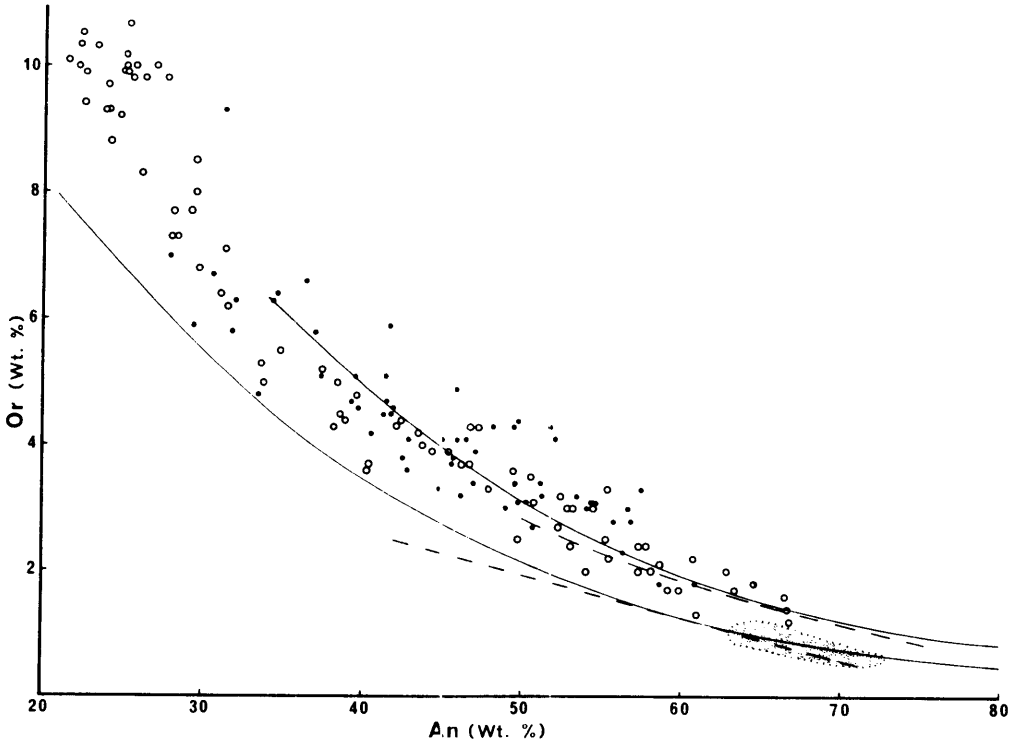

Fig. 5.25: Plot of Or content (wt %) against An content (wt %) of the plagioclases from the tholeiitic volcanics of the southern portion of the Tweed Shield. Open circles, plagioclase phenocrysts; filled circles, groundmass plagioclases. Generalized trends for plagioclases from the North and South Islands, Lake Rudolph, Kenya (lower and upper continuous lines respectively; Brown and Carmichael, 1971), the chilled upper and more slowly cooled central portions of the Makaopuhi lava lake, Hawaii (lower and upper dashed lines respectively; Evans and Moore, 1968) and Hawaiian tholeiitic lavas (stippled area; Keil *et al.*, 1972) are shown for comparison.

(Carmichael, 1963).

The close similarity of trends for various alkaline and subalkaline lavas plotted on Figure 5.25 indicates that previous suggestions that feldspars from alkaline rocks are inherently more potassic than those from tholeiitic rocks (Muir, 1962) are unjustified. However the plagioclases of alkaline rocks probably zone continuously to alkali feldspar compositions in contrast to the plagioclases from subalkaline rocks where zoning is more restricted (Keil *et al.*, 1972). This zoning probably explains the high Or contents of some sodic labradorites recorded in alkaline rocks (Wilkinson, 1965; Huckenholz, 1965).

In the light of this discussion a search for external factors controlling the Or contents of plagioclases e.g. volatile pressure and the rate of crystallization, (Evans and Moore, 1968; Brown and Carmichael, 1971) seems unnecessary. Provided the host liquids are sufficiently or-rich to fall within the two-feldspar field in the Ab-An-Or system (Smith and McKenzie, 1958; Tuttle and Bowen, 1958), the Or content will be determined simply by the intersection of the solidus and solvus curves within this system. External factors control the position of this intersection only insofar as they affect the position of the solidus and solvus curves.

iii) Iron Contents of Plagioclase

Figure 5.26 is a plot of total Fe versus An content for plagioclase feldspars in lavas of both series. It has been customary to assume that most of the Fe in terrestrial plagioclase is substituting for Al in tetrahedral sites and Fe has accordingly been calculated as Fe_2O_3. For clarity of presentation average Fe_2O_3 contents over 5% An intervals for phenocrysts

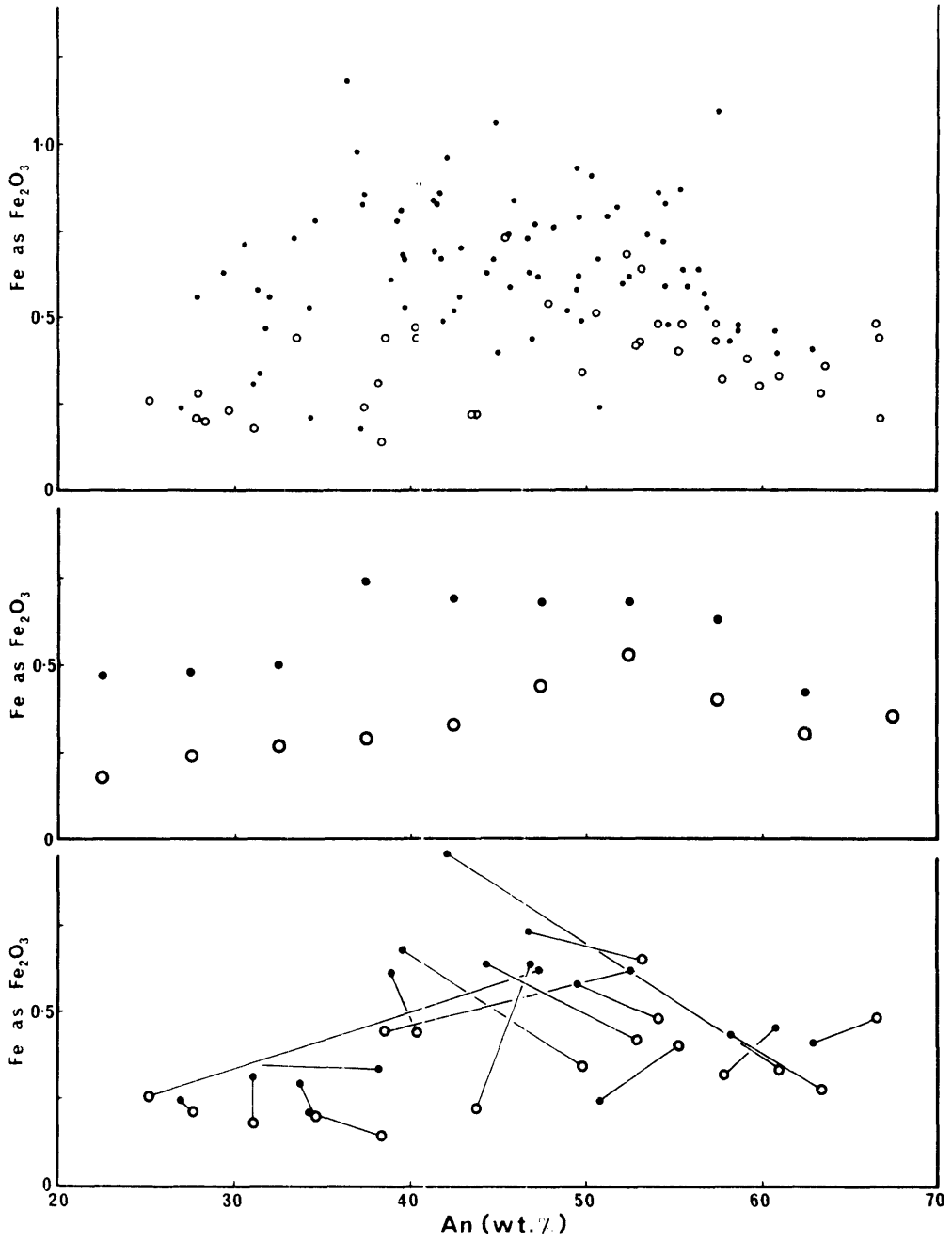

Fig. 5.26: Plot of Fe (as wt % Fe_2O_3) against An content (wt %) of plagioclases from tholeiitic rocks of the southern portion of the Tweed Shield. Open circles, interior portions of plagioclase phenocrysts; filled circles, phenocryst rim and groundmass plagioclases. Upper diagram, all analyses; middle diagram, groups of analyses averaged over intervals of 5 wt % An; lower diagram, cores and margins of phenocrysts, joined by tie-lines.

and groundmass grains are also plotted together with core-margin trends for individual crystals. Several features of the Fe content of plagioclase may be summarized from the microprobe data and this diagram.

(1) There is no essential difference in the Fe_2O_3 content of feldspars of a given composition in rocks of the two series.

(2) Fe_2O_3 is significantly higher in groundmass grains and phenocryst margins than in the interior of phenocrysts. A similar trend is evident in plagioclase from various submarine basalts (Bryan, 1972).

(3) The iron content reaches a maximum in intermediate plagioclases (An_{40} to An_{55}) and decreases with increase and decrease in An from these values. A similar trend is observed in feldspars in alkaline lavas of the Lake Rudolf region of East Africa (Brown and Carmichael, 1971)

(4) Increase in Fe_2O_3 at phenocryst margins occurs regardless of whether zoning is normal or reversed.

(5) Fe_2O_3 is virtually absent from the plagioclases of rhyolitic rocks.

Brown and Carmichael (1971) discuss several factors which may affect entry of Fe^{3+} into plagioclase, including the effects of crystallization temperature, rate of crystallization, volatile pressure (notably P_{H_2O}) and the ability of the plagioclase structure to accept Fe^{3+}. Another variable, namely the availability of Fe^{3+} in the host liquid is undoubtedly an important determinant in the essentially Fe-free plagioclases from rhyolites.

More An-rich plagioclase should favour entry of Fe^{3+} at the expense of the smaller Al^{3+} ion into tetrahedral sites since the tetrahedral

Al-O bond length of plagioclase is greater in anorthite than in Ab-rich feldspars. This is at variance with the decreasing Fe^{3+} in the most An-rich plagioclases. On this basis Brown and Carmichael (1971) reject ability of the plagioclase structure to accept Fe^{3+} as a major factor controlling Fe^{3+} in plagioclase, and they conclude that crystallization temperature is probably an important control. However it suffers from the same shortcoming as the first factor in failing to explain the decrease in iron in the most calcic plagioclases. Furthermore their data do not discriminate between phenocryst and groundmass analyses. The significant increase in Fe_2O_3 from phenocrysts to groundmass shown in Figure 5.26 is not in accordance with their hypothesis.

The phenocryst-groundmass trend is obviously highly significant with respect to the rate of crystallization. Concentration gradients exist in magmatic liquids around growing plagioclase phenocrysts (Bottinga *et al.*, 1966). Thus liquid immediately adjacent to the interface between a growing plagioclase and the host liquid is enriched in Fe relative to the bulk liquid. It is therefore reasonable that Fe^{3+} should be enriched in groundmass grains and phenocryst margins formed during rapid chilling. Marginal iron enrichment in phenocrysts regardless of whether zoning is normal or reversed strongly supports this argument.

Assessment of the influence of volatile pressure on the entry of Fe^{3+} into plagioclase is exceedingly difficult. However since it is believed that volatile pressures prior to and during extrusion were low, their effects have probably been minimal. Volatile pressure (especially P_{H_2O}) is likely to have been lower during crystallization of phenocryst

margins and groundmass plagioclase following extrusion, compared with the earlier phase of intratelluric crystallization. Therefore if volatile pressure has controlled entry of Fe^{3+} its effect has apparently been to suppress rather than to enhance the substitution.

iv) Feldspar Geothermometry

Kudo and Weill (1970) have developed an empirical geothermometer based on the composition of plagioclase and its host liquid. Numerous workers have since applied this geothermometer to volcanic rocks to obtain estimates of temperatures of extrusion (Stormer and Carmichael, 1971; Brown and Carmichael, 1971; Ewart *et al.*, 1971; Bauer *et al.*, 1973).

Several limitations to the application of this geothermometer have been discussed by later workers. These are:

(1) Estimated extrusion temperatures often appear excessively high, particularly in more basic rocks (Brown and Carmichael, 1971; Mathez, 1973).

(2) Plagioclase compositions are strongly dependant upon P_{H_2O} (Yoder, 1969a,b).

Different equations were derived by Kudo and Weill for 0, 0.5, 1.0 and 5.0 kb P_{H_2O} to compensate for this effect. However quantitative evaluation of P_{H_2O} is rarely possible unless some H_2O buffer system is present (e.g. the sanidine-magnetite-biotite-water-O_2 buffer; Wones and Eugster, 1965).

(3) The opposing effect of increased dry load pressure during intratelluric crystallization immediately preceding eruption is disregarded.

(4) The degree of subsolidus re-equilibration is indeterminable although this is probably negligible in volcanic rocks.

(5) The calculated temperatures, particularly those for acid rocks, will be quite sensitive to selective leaching of sodium during hydration of glasses or devitrification (Lipman, 1965; Noble, 1967). Apparently low values of Na_2O for whole rocks or residual glasses (as suggested by normative corundum) will lower the calculated temperatures of extrusion.

With these limitations in mind crystallization temperatures have been calculated using plagioclase phenocryst core compositions (or groundmass plagioclase compositions where phenocrysts are absent) and whole rock chemical data. The possible effects of high load pressure have been minimized by using only normally zoned, unsieved phenocrysts. Microprobe data have been used and where this is not available, compositions of the most calcic phenocrysts have been derived from measurements of the β refractive index. Since microprobe Na_2O determinations on the residual glasses are apparently low (Section 5.6) it has not been possible to obtain estimates of the lower temperature limits of plagioclase crystallization.

Calculated crystallization temperatures are plotted in Figure 5.27 against Mafic Index. This parameter has been selected because of its close relationship to liquidus temperatures determined at atmosphere (Tilley *et al.*, 1963,1964,1965; Thompson and Tilley, 1970; Thompson, 1972a). It must be emphasised that the plotted temperatures can only be equated with the temperature of first appearance of plagioclase during melting studies. In most Tweed lavas however it seems likely that plagioclase has been the

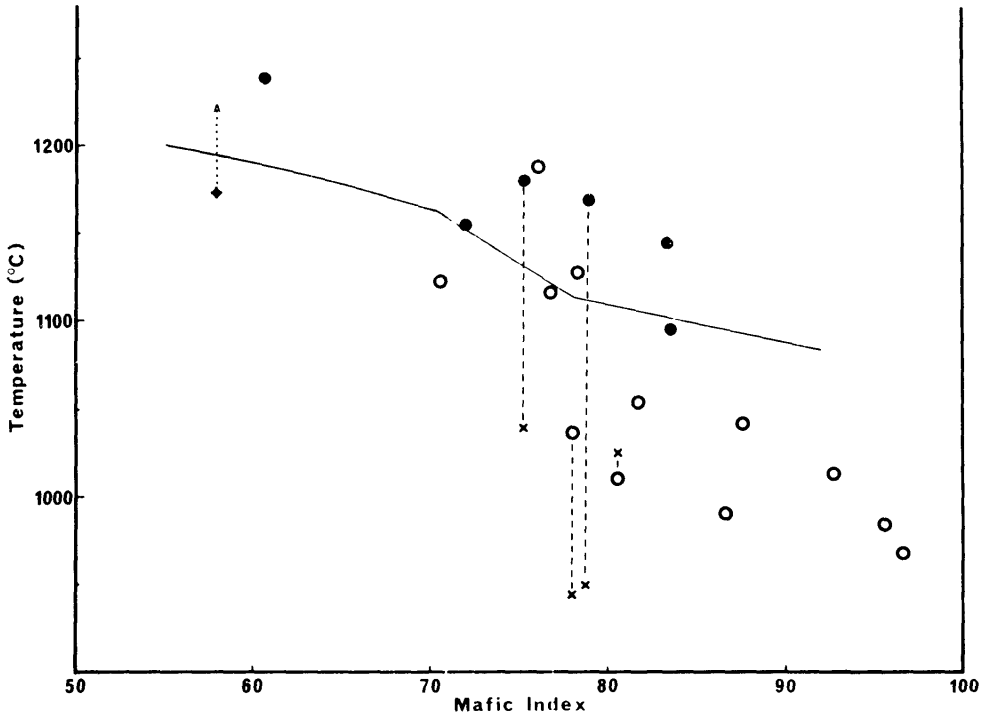

Fig. 5.27: Crystallization temperatures of plagioclase calculated using the Kudo-Weill plagioclase geothermometer (filled circles, rocks of the low-Si series; open circles, rocks of the high-Si series; ✦, most mafic low-Si tholeiitic andesite containing groundmass plagioclases only) and the Fe-Ti oxide geothermometer (crosses) against Mafic Index. Continuous line denotes the generalized trend for experimentally determined 1 atmosphere liquidus temperatures for the Snake River lavas, Idaho (Tilley and Thompson, 1070).

liquidus phase under low pressure near-surface conditions. An exception would be the most mafic low-Si tholeiitic andesite 28046 where olivine phenocrysts are abundant but plagioclase is confined to the groundmass. The calculated temperature in this case may be considerably lower than the actual liquidus temperature.

A general trend of decreasing liquidus temperatures with iron enrichment is immediately apparent. Furthermore the data strongly suggest that there is overall a finite difference between the initial temperatures at which plagioclase first appears in the low-Si and the high-Si series at an equivalent M.I., the latter being lower by some 50-150°C. This may reflect the significantly higher levels of silica saturation in the high-Si series. Alternatively it may reflect increased water pressures during intratelluric crystallization in the more Fe-enriched members of the low-Si series. It has already been noted that in the most Fe-rich of these rocks titanomagnetite appears in place of ilmenite as the sole opaque oxide phase.

Temperatures have also been obtained for two rocks of the low-Si series and one of the high-Si series using the Fe-Ti oxide geothermometer of Buddington and Lindsley (1964) (see Section 5.3). Since the Fe-Ti oxides in these particular rocks are late in the crystallization sequence, the derived temperatures probably approximate to the solidus temperatures. If the Kudo-Weill temperatures approximate to liquidus temperatures, estimates of the crystallization interval are possible. Estimates of these accord quite well with 1 atmosphere melting data on volcanics with comparable compositions and with observed petrographic relationships. One low-Si tholeiitic andesite (28051; crystallization interval ~220°C) contains only a trace of rhyolitic

residual glass and should therefore display a near maximum crystallization interval. The calculated interval does not appear unreasonable. For example, Yoder and Tilley (1962) suggest a crystallization interval of 150-200°C for most basaltic lavas and Brown and Carmichael (1971) deduce intervals of 250-300°C by this method for some Lake Rudolf (Kenya) alkaline lavas. Another low-Si tholeiitic andesite (28050) contains small crystals of olivine and plagioclase, but not clinopyroxene, and abundant iron-charged residual material (approx. 50 vol. %). Its crystallization has therefore been arrested by rapid chilling subsequent to eruption and a smaller crystallization interval (calculated interval ~140°C) would therefore be expected. Similarly for 28063, a high-Si tholeiitic andesite also containing abundant residual glass, the calculated crystallization interval is quite low (~90°C). For another rock (28067) a less reliable Fe-Ti oxide temperature (obtained on an ilmenite phenocryst and magnetite included in olivine) more likely represents a near liquidus temperature (Section 5.3); for this particular volcanic the plagioclase temperature approximates to the Fe-Ti oxide temperature.

5.5 ACCESSORY MINERALS

i) Biotite

Biotite is almost totally absent as a phenocryst phase in rocks of the Tweed Shield. However, a microprobe analysis of one small biotite grain included in sanidine (Plate 5, No. 3) in a rhyolitic pitchstone (28078) has been obtained and this analysis is listed in Table 5.7 together with a structural formula calculated anhydrous on the basis of 22 oxygen atoms. The biotite, more strictly an annite, has a high 100 Fe/Fe+Mg ratio (78.2) which reflects the low MgO content of the host rock (0.05%).

TABLE 5.7

MICROPROBE ANALYSES OF BIOTITE INCLUDED IN SANIDINE IN RHYOLITIC PITCHSTONE (28078)

		Structural formula on the basis of 22 oxygen atoms (anhydrous)		
SiO_2	34.94	Si	5.464)	
TiO_2	7.69	Al	2.477)	8.00
Al_2O_3	13.44	Ti	0.059)	
FeO	27.73	Ti	0.845)	
MgO	4.34	Fe	3.626)	5.48
Na_2O	0.19	Mg	1.011)	
K_2O	8.84			
Total	97.17	Na	0.057)	1.82
Mol. 100 Fe/Fe+Mg = 78.2		K	1.763)	

Despite the rarity of biotite as a primary phenocryst phase, it quite commonly forms ragged groundmass granules in microcrystalline rhyolites where it may have developed during devitrification or else have precipitated directly from the melt in the more slowly cooled and probably more hydrous central portions of thick rhyolite flows.

ii) Allanite

Extremely rare microphenocrysts of allanite, never exceeding 0.5 mm in diameter, occur in some vitric rhyolites and pyroclastics. Optical properties are typical of non-metamict allanite with X = light brown; Z = dark brown and γ ~1.75.

Partial microprobe analyses of two allanites and X-ray diffraction

data are set down in Table 5.8. The electron microprobe was not programmed to analyse for rare earth elements which substitute for Ca in allanite (Deer, Howie and Zussman, 1962). However, the energy dispersive detector system coupled to a multichannel analyser enabled very approximate estimation of principal rare earth abundances by measurement of L_α radiation peak heights for the allanite in 28078. These include La_2O_3 (~11%), Ce_2O_3 (~7%), Sm_2O_3 (~3%) and Gd_2O_3 (~2%). Trace amounts of other rare earths are probably present.

A characteristic accessory mineral in many granitic rocks and especially pegmatites, allanite is quite rare in volcanic rocks. Trace amounts occur widely distributed in ash fall and ash flow tuffs of the western United States (Izett and Wilcox, 1968) and Northern Queensland (Branch, 1966), but it has not been described from lavas. Its occurrence in Tweed vitric rhyolites as microphenocrysts and included in sanidine (Plate 5, No.3) is therefore of special interest and attest to its undoubted early crystallization directly from an acid melt. This contrasts with its common occurrence in pegmatites where it has been interpreted as a late stage auto-pneumatolytic mineral (Tröger, 1967).

iii) Zircon

Minute euhedra of zircon (~0.05 mm) occur in all rhyolitic rocks where they are commonly closely associated with ilmenite and ferrohypersthene or its breakdown products.

5.6 RESIDUAL GLASS

Most tholeiitic rocks of both series are characterised by the

TABLE 5.8

PARTIAL MICROPROBE ANALYSES AND X-RAY DIFFRACTION DATA ON ALLANITES

	1	2		a		b	
				d(A)	I/I_o	d(A)	I/I_o
SiO_2	29.2	29.4	1	9.19	30	9.2	40
TiO_2	2.3	1.6	2	8.04	30	8.0	40
Al_2O_3	12.6	13.5	3	5.09	5	5.11	20
FeO*	17.7	17.3	4	4.66	5	4.72	20
MnO	0.63	0.48	5	3.80	1	3.78	10
CaO	10.1	10.8	6	3.53	40	3.53	50
			7	3.30	30	3.32	20
			8	3.16	60	3.23	20
*Total Fe as FeO			9	2.92	100	2.92	100
			10	2.70	40	2.71	60
			11	2.62	30	2.63	50
			12	1.64	20	1.639	50

1. Allanite partially included in sanidine in rhyolitic pitchstone 28078 (Table 6.3, Anal. 4; Plate 5, No.3).

2. Allanite microphenocryst in rhyolitic pitchstone 28079 (Table 6.3, Anal. 5).

a. X-ray diffraction data (powder photo; 12 strongest lines) on a composite sample of allanite separated from several rhyolitic pitchstones from the Tweed Shield. I/I_o - visual estimation.

b. X-ray diffraction data on allanite from the Guaje Pumice Bed, Cañones, New Mexico (Izett and Wilcox, 1968). Twelve lines corresponding to those listed for the Tweed allanite (column a).

presence of small amounts of residual glass whose abundance is to some extent a function of host rock composition. Thus rocks of the high-Si series and more evolved members of the low-Si series contain substantially more glass than mafic members of the low-Si series. In the low-Si series glass only becomes evident as intersertal isotropic patches where crystallization had proceeded almost to completion before quenching. In other less crystallized rocks an opaque-charged residuum is abundant. By anlogy with similar tholeiites in the Inverell area, New South Wales (Wilkinson and Duggan, 1973) these residua are probably andesitic in composition, relatively more evolved than their respective host rocks.

Many rocks bearing small amounts of residual glass have areas sufficiently large and free of inclusions to enable microprobe analysis. The results of several such analyses are listed in Table 5.9. The usefulness of microprobe data on rock glasses is limited by two important factors. Firstly, residual glasses are rather heterogenous in character with substantial compositional variation occuring over small distances. Accordingly, analyses reported in Table 5.9 represent averages of at least 4 determinations on different points. Secondly, and more importantly, extensive volatilization of Na by the electron beam will produce an erroneously low Na_2O value, even with the relatively low accelerating voltage and specimen current employed in the microprobe analysis (see Appendix I). Thus Na_2O values are unrealistically low when asses in conjunction with host rock composition and the nature of its constituent crystalline phases. An exception is the evolved icelandite 28072 in which areas of glass are sufficiently large to permit defocussing of the electron beam and thus avoid extensive volatilization of Na. C.I.P.W.

TABLE 5.9

MICROPROBE ANALYSES OF RESIDUAL GLASSES

	1	2	3	4	5	6	7	8	9	10
SiO_2	74.00	73.54	74.33	73.88	73.27	74.21	71.25	74.26	74.37	74.51
TiO_2	0.99	1.05	0.84	0.76	0.65	0.26	0.27	0.22	-	-
Al_2O_3	12.44	14.94	11.94	13.68	13.33	13.30	14.14	14.33	13.26	13.15
FeO*	1.84	1.95	2.82	1.05	1.07	1.20	2.53	1.53	1.08	0.39
MgO	-	0.07	0.12	-	-	-	0.06	-	-	-
CaO	0.31	0.36	0.41	0.26	0.21	0.37	0.84	0.51	0.51	0.46
Na_2O	(2.3)	(1.8)	(1.2)	(1.6)	(0.9)	(1.6)	(3.75)	(1.3)	(1.6)	(1.5)
K_2O	4.64	4.33	5.54	6.25	6.40	5.91	5.38	5.26	5.25	5.15
Total	96.54	97.98	97.23	97.49	95.82	96.82	98.22	97.38	96.06	95.23

KEY TO TABLE 5.9

1. Residual glass (grey) in low-Si tholeiitic andesite 28048 (Table 6.1, Anal.3).
2. Residual glass (grey) in low-Si tholeiitic andesite 28049 (Table 6.1, Anal.4).
3. Residual glass (brown) in low-Si tholeiitic andesite 28051 (Table 6.1, Anal.6).
4. Residual glass (grey) in high-Si tholeiitic andesite 28061 (Table 6.2, Anal.1).
5. Residual glass (grey) in icelandite 28070 (Table 6.2, Anal.10).
6. Residual glass (brown) in icelandite 28071 (Table 6.2, Anal. 11).
7. Residual glass (brown) in icelandite 28072 (Table 6.2, Anal. 12).
8. Residual glass (brown) in rhyodacite 28073 (Table 6.2, Anal. 13).
9. Residual glass (brown) in rhyolitic pitchstone 28079 (Table 6.3, Anal. 5).
10. Residual glass (clear) in rhyolitic pitchstone 28079.

* Total Fe as FeO.

norms have not been calculated for the glasses as these are virtually meaningless in the absence of reliable Na_2O determinations.

The above limitations notwithstanding, it is immediately apparent that the residual glasses are typically rhyolitic in overall chemistry. In fact they closely resemble the rhyolitic rocks of the Shield apart from a significantly higher TiO_2 content. However this feature is less marked in members of the high-Si series where removal of ilmenite as a phenocryst phase has caused early depletion of TiO_2 in the residual liquid. The close chemical similarity between these residual glasses and the rhyolites (which will be interpreted as products of fractionation at intermediate crustal depths) demonstrates that the ultimate product of fractionation of an oversaturated tholeiite magma may be essentially similar over a range of pressure conditions, namely a rhyolitic liquid broadly appropriate to the low temperature trough in "petrogeny's residua system" (Ab-Or-Qz).

In many rhyolitic pitchstones of the Shield two distinct types of glass are found, often side by side. One type is brown and crystal-free while the other is clear but charged with microlites. The two types have been analysed with the microprobe in one rhyolite (28079; Table 5.9, Nos 9 and 10). Not surprisingly, the brown variety is significantly more Fe-rich than the clear type. However in other respects the two varieties are virtually identical.

Two residual glasses from phenocryst-rich rhyolites have been separated for complete major element analysis. The data on these glasses are presented in the following chapter where their chemistry can be assessed more fully in relation to that of their respective host rocks.